

A Rule-Based Classification Method for Mapping Saltmarsh Land-Cover in South-Eastern Bangladesh from Landsat-8 OLI

Sheikh Mohammed Rabiul Alam & Mohammad Shawkat Hossain

To cite this article: Sheikh Mohammed Rabiul Alam & Mohammad Shawkat Hossain (2020): A Rule-Based Classification Method for Mapping Saltmarsh Land-Cover in South-Eastern Bangladesh from Landsat-8 OLI, Canadian Journal of Remote Sensing, DOI: [10.1080/07038992.2020.1789852](https://doi.org/10.1080/07038992.2020.1789852)

To link to this article: <https://doi.org/10.1080/07038992.2020.1789852>



Published online: 11 Jul 2020.



Submit your article to this journal 



Article views: 83



View related articles 



View Crossmark data 



A Rule-Based Classification Method for Mapping Saltmarsh Land-Cover in South-Eastern Bangladesh from Landsat-8 OLI

Une méthode de classification fondée sur des règles pour cartographier les marais salés dans le sud-est du Bangladesh à partir de Landsat-8 OLI

Sheikh Mohammed Rabiul Alam  and Mohammad Shawkat Hossain 

Institute of Oceanography and Environment (INOS), Universiti Malaysia Terengganu (UMT), 21030 Kuala Nerus, Terengganu, Malaysia

ABSTRACT

Wetland vegetation classification often treated the saltmarsh as a single type of land-cover (LCT). Mapping the dynamic and spatially complex coastal zones using optical remote sensing is still challenging. This study firstly analyzed the spectral properties of target objects generated by Landsat 8 (OLI), formulated new spectral indices and then proposes a rule-based approach to mapping five vegetated (saltmarsh, seagrass, mangrove, non-mangrove forest, and agricultural land) and three non-vegetated (wet sand, saltpan, and built-up areas) LCT in the study area, that is, large coasts located in the south-eastern coasts of Bangladesh. The thresholds of spectral indices were selected from the newly introduced spectral indices over the method development site (Bakkhali estuary). The rule-based LCT classification process followed a set of cascade rules of image thresholding and masking, based on a hierarchical tree in order to generate detailed thematic maps of saltmarsh land-cover. Overall accuracy (OA) and Kappa coefficient (K) of rule-based approach were 84.6% and 0.821, respectively. The reliability and robustness of the approach was tested over two independent external validation test sites: Karnaphuli river estuary and Teknaf peninsula and consistent accuracy results achieved: OA = 81.7% (K = 0.787) and OA = 84.6% (K = 0.821) respectively.

RÉSUMÉ

Les classifications de la végétation des terres humides traitent souvent le marais salé comme un seul type de couverture terrestre (LCT). Il est encore difficile de cartographier les zones côtières dynamiques et spatialement complexes à l'aide de la télédétection optique. Cette étude a d'abord analysé les propriétés spectrales des objets cibles générés par Landsat 8 (OLI) et formulé de nouveaux indices spectraux. Ensuite, elle propose une approche basée sur des règles pour cartographier cinq zones végétales (marais salés, herbes marines, mangroves, forêts et terres agricoles) et trois zones non végétalisées (sables humides, salines et zones construites), d'une grande région côtière du sud-est du Bangladesh. Les seuils des indices spectraux ont été choisis à partir des indices spectraux nouvellement introduits sur le site de développement de la méthode (l'estuaire de Bakkhali). Le processus de la classification LCT a appliqué un ensemble de règles de seuillage et de masquage en cascade, basées sur un arbre hiérarchique afin de générer des cartes thématiques détaillées des marais salés. L'exactitude globale (OA) et le coefficient Kappa (K) de l'approche de classification proposée est de 84.6% et de 0.821 respectivement. La fiabilité et la robustesse de l'approche ont été testées indépendamment sur deux autres sites de validation: l'estuaire de la rivière Karnaphuli et la péninsule de Teknaf. Des précisions similaires ont été obtenues pour les deux sites, soient OA = 81.7% (K = 0.787) et OA = 84.6% (K = 0.821) respectivement.

ARTICLE HISTORY

Received 22 February 2020
Accepted 25 June 2020

Introduction

Saltmarsh communities are macrophytes, found mostly in the lower marsh, covering an estimated global area of 2.2 Mha–40 Mha (Pendleton et al. 2012).

Saltmarshes are distributed in large latitudinal areas under a variety of climatic conditions in the intertidal zone where generally muddy substrates support diverse halophytic plants (Davy 2000) and in places

where mangroves have limited occurrence (Kangas and Lugo 1990; West 1977). They provide enormous ecosystem services (Costanza et al. 1997) but often neglected the contribution toward livelihoods through the food supply, carbon and sediment storage, and flood control at a local scale, and regulate climate, provide habitat for associated species, and coastal protection at a global scale (Zedler and Kercher 2005; Mcowen et al. 2017). Despite their ecosystem services being recognized, saltmarsh cover continues to be lost at an unknown temporal rate. Globally, saltmarsh cover has declined at a rate of 1%–2% per year (Duarte et al. 2008; Crooks et al. 2011) due to known human activities, such as the conversion of land-cover to agriculture, and concentrated coastal development activities (Gedan et al. 2009).

In Bangladesh, varieties of coastal vegetation such as mangroves, saltmarshes, seagrass meadows, fisheries, and macro and micro-algae are sparsely distributed in subtidal and intertidal areas and semi-enclosed lagoons of about 710 km coastline of Bangladesh (Abu Hena et al. 2010). The Chakaria mangroves, saltmarshes, and seagrass meadows are mostly found in Cox's Bazar's eastern coastal and estuarine areas (Hossain 2001; Abu Hena et al. 2010). Local people are using saltmarsh as forage for cattle and stuffing. In Cox's Bazar's coastal and estuarine environments, crabs, crustaceans and mollusks use saltmarshes and seagrass meadows as critical nurseries. Unfortunately, because of known human activities such as over-extraction of resources, shrimp farming, destructive fishing activities, and agricultural practices, Bangladesh had already lost such ecologically and economically important saltmarsh resources at an unknown temporal rate and spatial extent/coverage (Hossain 2001). The geographic location and extent of saltmarsh land-cover aiming to generate wetland land use and coverage maps are poorly studied. With the continued increasing population pressure, urbanization, and coastal development activities on saltmarshes, reliable and timely information on present status, their distribution, and health are becoming increasingly important with a view to planting effective coastal management programs and biodiversity conservation strategies.

Most of the saltmarsh remote sensing researches used radar technologies to develop digital elevation models (Hladik and Alber 2012; van Beijma et al. 2014), to map halophytes including saltmarsh (Lee et al. 2012) or combined radar and optical remote sensing techniques to map distribution (Yeo et al. 2020) and biomass (Kulawardhana et al. 2014) over recent years. Radar is relatively less affected by atmospheric conditions and has the ability to capture

electromagnetic information of the target objects. However, until recently, the scarcity and cost of radar data are major shortcomings in mapping wetlands (Joshi et al. 2016). Another major challenge of analysis of radar data, particularly for accurately mapping land cover changes, is speckle which may degrade the radiometric quality of the image, increase uncertainty and yield map with poor classification accuracies (Maghsoudi et al. 2012). Optical remote sensing is hindered by the inability to penetrate through clouds. Multispectral remote sensing is unable to detect water available on the forest floor due to poor spectral penetration of the dense canopy (Gallant 2015). Similar spectral properties received by the sensor from the spectrally similar objects, which is a common issue in the saltmarsh environment, may also cause misclassification (Sun et al. 2018; Ouyang et al. 2013).

Mapping of saltmarsh resources requires reproducible and reliable updates of land-cover maps to assist wetland inventory. Remote sensing has excellent advantages in its larger spatial coverage compared to expensive, low coverage field measurements in areas with restricted accessibility (Xie et al. 2008). There are many high spatial or spectral (e.g., hyperspectral) saltmarsh-derived communities or species mapping products (William et al. 2003; Silvestri et al. 2003; Hestir et al. 2008; Hunter et al. 2010), but they are relatively expensive and less available compared to multispectral imagery of medium spatial resolution. Fortunately, these sensors provide opportunities to observe a wide coastal area and are freely available (Lira and Taborda 2014; Wang et al. 2018; Sun et al. 2016). Nevertheless, the high spectral similarity of different wetland species, coupled with an inability to detect patches of vegetation or land-cover type narrower than the spatial resolution of images such as Landsat (30 m), resulting in low accuracies for the classification of vegetation and other land-cover (Phiri and Morgenroth 2017). Some researchers have tested machine learning approaches, such as random forest, support vector machine for estimation and mapping of saltmarsh biomass, using Worldview-2 imagery (Rasel et al. 2019). Recently, machine learning tools, such as the weighted majority voting, Bayesian network learning, and K-neural network have been used in mapping blue carbon ecosystems, comprising of mangroves, salt marshes, and seagrasses (Pham et al. 2019).

Because of the high cost of acquiring high-resolution imagery such as Digital Globe's IKONOS and QuickBird, free accessible Landsat data is

preferred (Sun et al. 2018). Although hyperspectral remote sensing can provide spectral signatures to detect saltmarsh species and differentiate species, it is not suggested for routine large-scale mapping of coastal areas (Belluco et al. 2006). Landsat imagery has been applied in the monitoring of wetland and saltmarsh habitats due to their cost-effective way of acquisition. As a result of the Landsat Global Archive Consolidation (LGAC) initiative began in 2010 by the USGS, Landsat data coverage has improved (Wulder et al. 2016), resulting in an enhanced capacity for mapping global coastal wetlands (Murray et al. 2019). In the past, however, studies on saltmarsh land-covers using single coarse-resolution Landsat data have failed to achieve the required accuracy where classes are intermixed (Klemas 2013; Harvey and Hill 2001). To resolve the problem of mapping mixed halophytic vegetation, previous studies have demonstrated the potential for the application of neural network classifier for analyzing airborne hyperspectral imagery (Wang et al. 2007). Researchers had difficulties using low-resolution Landsat pixels for discriminating upper saltmarsh from the upland terrestrial forest (Civco et al. 2006). Whether the high or moderate multispectral resolutions used in mapping, spatial heterogeneity may make the classification of imagery with required accuracy challenging.

For a suitable method for mapping saltmarsh land-cover, existing methods have been tested in the homogenous regions (Zhang et al. 1997) rather than in complex coastal vegetation where saltmarsh, mangrove, and terrestrial vegetation co-occur. Spectral indices based on vegetation, soil, or water characteristic variables alone cannot provide the information required to discriminate target classes of interest for mapping detailed thematic mapping of natural coastal areas. Discriminating mangrove from non-mangrove vegetation using multispectral remote sensing is still challenging as evident in recent researches (Gupta et al. 2018; McCarthy et al. 2015). For classification of coastal above-ground vegetation researchers commonly utilized information from the different types of vegetation indices (VI), of which the Normalized Difference Vegetation Index (NDVI) is the most popular one. The formulation of monthly NDVI is also found useful for the classification of low, upper low, and high saltmarsh (Sun et al. 2018). However, the selection of the best index is not an easy process. Previous studies have compared simple VI, Atmospheric resistance VI, Soil adjusted VI and other potential VIs to discriminate saltmarshes mostly using high-resolution images (Belluco et al. 2006; Timm and

McGarigal 2012) and to a lesser extent using moderate resolution images such as Landsat (Zhang et al. 1997; Lopes et al. 2019), with varying levels of accuracies. Some consider that selection of appropriate thresholds may help the identification of target classes (Kantakumar and Neelamsetti 2015). The selection of suitable band or combination of bands of moderate resolution imagery to formulate spectral indices is not predefined in mapping saltmarsh habitat and requires analysis to determine which combination is appropriate to separate target classes of interest. The ability of Landsat to map land-cover types has not been extensively tested in the saltmarsh environment.

This study explores the potential of Landsat for reliably discriminating saltmarsh land-cover types (LCT) integrated with field observations. Given the growing interest of resource managers and remote sensing practitioners in spatially heterogeneous, estuary-wide inventory of saltmarshes, this study developed a rule-based approach involving image normalization, band ratio techniques, and selection of spectral thresholds and classified dominant LCTs across the coasts of Bangladesh as a case. The objective of this study was to propose a spectral index threshold—a class-specific saltmarsh LCT detection index that would allow describing the coastal land-use and cover, that is, saltpan, built-up area, near-shore coastal wetland habitat, for remote sensing of coastal vegetated and un-vegetated areas from space and accurate mapping the status and distribution of coastal resources. Our approach is simple, transparent, and easily updateable and transferable, enabling the coastal managers to readily access mapped data.

Materials and methods

Study sites

The saltmarsh habitats chosen for the development and validation of the above mentioned rule-based method, namely the Karnaphuli river estuary (marked with L1 in Figure 1), the Bakkhali river estuary (marked with L2 in Figure 1), and the Teknaf peninsula (marked with L3 in Figure 1) are located in the southern coasts of Bangladesh, with significant variations in the spatial distribution and pattern of saltmarsh patches, coexistence of other vegetation such as mangroves and terrestrial forests. In order to develop the rule-based classification method where all target classes of interest were present, the location L2 was studied. The other 2 sites (marked with L1 and L3 in Figure 1) were used to investigate the robustness of the suggested method. There were significant

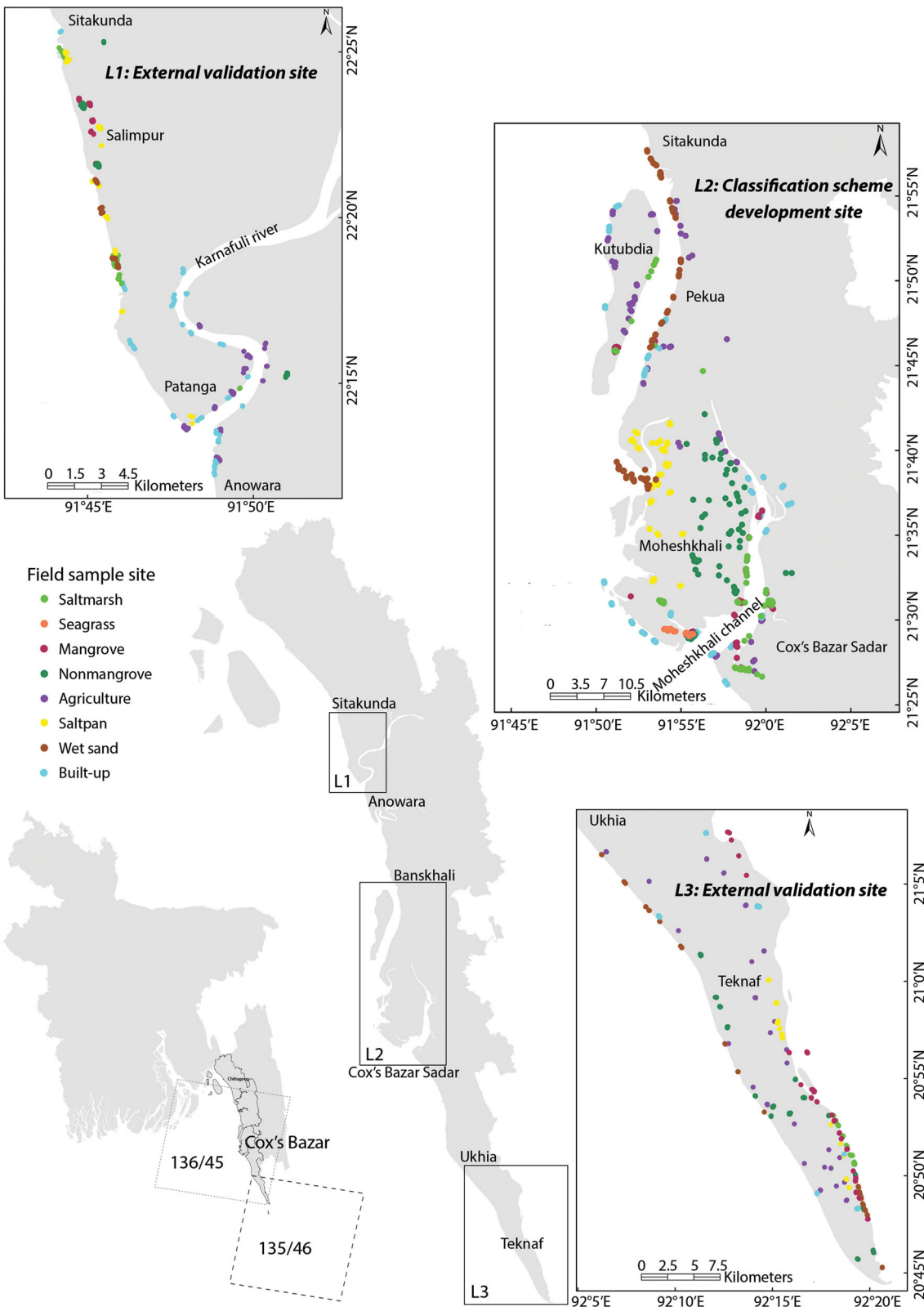


Figure 1. Location of study sites along with field data collection sites; L2 was chosen for developing the saltmarsh land-cover classification scheme and L1 and L3 were chosen for validation of the method.

Table 1. Species composition and environment of the three study sites.

	Species			Environment	
	Mangrove	Saltmarsh	Seagrass	Tide Type	Soil Type
Method validation site: Karnaphuli river estuary (L1)	<i>Sonneratia apetala</i> Buch.-Ham, <i>Avicennia marina</i> (Forsk.) Vierh. and <i>Acanthus ilicifolius</i> L.	<i>Porteresia coarctata</i> (Roxb.) Tateoka	Not present	Semidiurnal; tide height ranges from 1.1 to 4.5 m	Sandy clay
Method development site: Bakkhali river estuary (L2)	<i>Avicennia alba</i> Blume. A. <i>marina</i> (Forsk.) Vierh., <i>Acanthus ilicifolius</i> L., <i>Aegialitis rotundifolia</i> Roxb., and <i>Sonneratia apetala</i> Buch.-Ham.	<i>Imperata cylindrica</i> (L.) P. Beauv., <i>Porteresia coarctata</i> Tateoka, and <i>Spartina</i> sp.	<i>Halophila beccarii</i> Ascherson	Semidiurnal; tide height ranges from 0.07 to 4.4 m	Muddy and sandy
Method validation site: Teknaf Peninsula (L3)	<i>Sonneratia apetala</i> Buch.-Ham., and <i>Avicennia</i> sp.	<i>Porteresia coarctata</i> (Roxb.) Tateoka	Not present	Semidiurnal; tide height ranges from 2.5 to 4.42 m	Sandy and non-calcareous alluvium

differences in wetland species communities and environmental characteristics among the 3 study sites (**Table 1**).

The Karnaphuli river estuary (L1) is characterized by tertiary geological rocks (Rizbi 1971), located in the south-east of Chittagong port (between 22°12'–22°26' N and 91°42'–91°51' E) and the climate is influenced by the seasonal fluctuations of Indian monsoon (Alam and Zafar 2013). The intensity of built-up areas, covered by industries and factories, is relatively high around L1 (Das et al. 2002). This study conducted in about 55,282 ha that extends from Shitakunda to Anowara upazila, which is exposed to semi-diurnal tides (Lara et al. 2009). Temperatures range from 7.7°C during winter to 39.5°C during summer (Sharifuzzaman 1988). Saltmarshes are distributed over alkaline substrates of the estuary and they co-occur with mangroves (**Table 1**). Some micro-algae, namely *Ulva intestinalis*, *Catenella nipae*, and *Dictyota dichotoma* are found sporadically in mangrove stands.

The Bakkhali estuary (L2), located in the south-eastern coast (extending from Banskhali to Cox's Bazar sadar upazila; between 21°23'–21°57' N and 91°45'–92°3' E) is one of the largest estuaries in Bangladesh (**Figure 1**). This study covered about 190,220 ha where patches of saltmarsh, *Avicennia* dominated mangroves, and mono species of seagrass are distributed in the intertidal and subtidal mudflats (**Table 1**). The wetland vegetation receives terrestrial runoff through numerous water channels. The land-cover is heavily influenced by human influences including coastal reclamation, aquaculture activities, and construction of saltpan (Rashed-Un-Nabi et al. 2011). The terrestrial vegetation is commonly found around human habitation.

Another site located in the south-eastern border of Bangladesh (between 20°43'–21°7' N and

92°5'–92°21' E, with areal coverage of about 122,633 ha) was chosen as a test site given the spatial heterogeneity of saltmarsh land-cover around L3 (**Figure 1**). Non-calcareous alluvium mudflats support saltmarshes in Teknaf Peninsula (**Table 1**). The site is characterized by hilly areas on the north, the Naf river on the east, and the Bay of Bengal on the south and on the west. Huge numbers of canals and tributaries and streams across the wetland areas often causing floods during the rainy season (Chowdhury et al. 2011). Using the saline water of the Naf river, saltfans are built that help the local people running such a profitable business. Ecologically, the peninsula plays a significant role by hosting globally threatened marine turtles (Jafar et al. 2013), more than 80 different migratory birds, and feeding ground of marine mammals (Irrawaddy and Bottlenose dolphins) (Department of Environment 2015). Mangroves in Sonadia Island are highly salinity tolerant, but they are the last remaining forest under continued destruction caused by the forest-dependant people (Roy et al. 2019).

Field data collection

For deciding the saltmarsh land-cover mapping targets, saltmarshes, and associated vegetation type was first defined based on their dominance in terms of spatial coverage and interaction with the wetland ecosystem. A total of 1,323 field data were collected from the study sites L1 and L2 in December 2017 and 406 field data were collected from the study site L3 during the period of June–July 2016. The site L2 and its surrounding is a typical association of vegetation where mangrove, non-mangrove, seagrass, saltmarsh, and agricultural crops coexist (**Figure 2**). **Table 2** summarizes the different LCTs used in the present study. These field pieces of evidence have been also shown

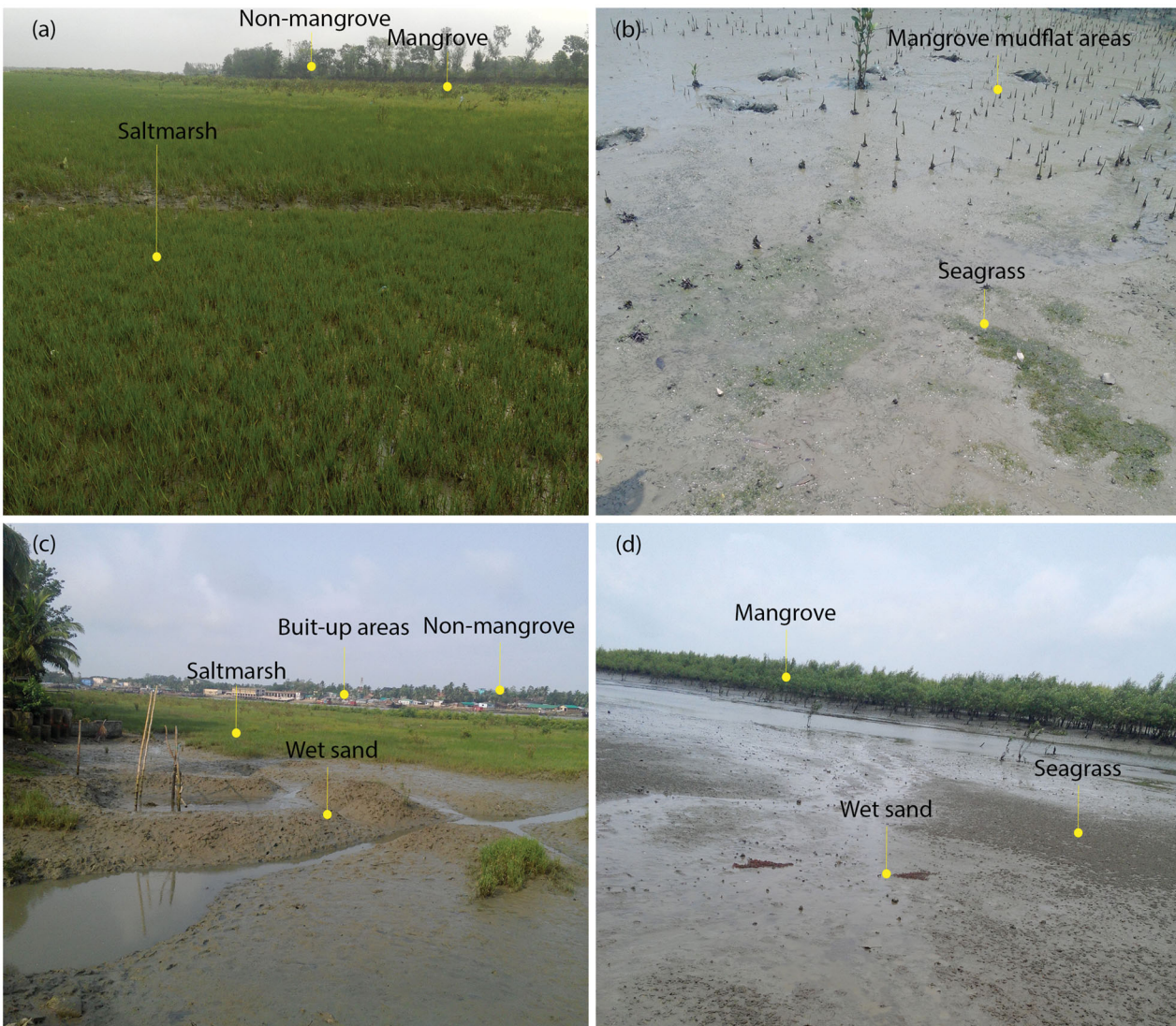


Figure 2. Some field photos, illustrating co-existence of saltmarsh with (a) non-mangrove, (b) seagrass, (c) scattered and (d) dense mangrove forests; (b-d) unvegetated mudflat and built-up areas are also present in the saltmarsh vegetation.

Table 2. Summary of characteristics of the land-cover types over the saltmarsh-wetland ecosystem.

Land-Cover Class	Description
Saltmarsh (SM)	<ul style="list-style-type: none"> Presence of SM vegetated portions of intertidal mudflats Species (herbs, shrubs and grasses) adapted to a wide range of salinity and to immersion by tides Deposition of deep mud and soft sediments
Seagrass (SG)	<ul style="list-style-type: none"> Presence of seagrass meadows or patches in gentle slopes in the protected shorelines
Mangrove (MF)	<ul style="list-style-type: none"> Presence of shrub and woody vegetation in the tidal mudflats Exposure of pneumatophores
Non-mangrove (NMF)	<ul style="list-style-type: none"> Presence of woody terrestrial vegetation other than mangroves (as also opposed to saltmarsh)
Agriculture (AL)	<ul style="list-style-type: none"> Cultivated areas covering crops including existing fallow lands
Saltpan (SP)	<ul style="list-style-type: none"> Areas used by salt farmers for salt cultivation by solar evaporation process of sea water.
Wet sand (WS)	<ul style="list-style-type: none"> Evidences of patches of mud $\geq 1 \text{ m}^2$ within saltmarsh vegetated portion, excluding mud on creek banks at elevations lower than saltmarshes
Built-up areas (BA)	<ul style="list-style-type: none"> Areas under rural and urban habitations including artificial facilities, homestead and industrial areas.

Table 3. Field data of saltmarsh LCT classes used for training and validating of classification, expressed in number of pixels on the Landsat OLI.

Class	Training Data			Validation Data		
	Karnaphuli River Estuary (L1)	Bakkhali Estuary (L2)	Teknaf Peninsula (L3)	Karnaphuli River Estuary (L1)	Bakkhali Estuary (L2)	Teknaf Peninsula (L3)
SM	26	65	19	26	60	19
SG	np	15	np	np	16	np
MF	40	65	45	25	54	30
NMF	50	65	45	35	65	30
AL	40	65	26	40	63	26
SP	30	65	25	25	34	30
WS	28	65	22	22	44	27
BA	35	65	31	35	60	31
Total	249	470	213	208	396	193

External validation data are in bold. The class abbreviations are as in Table 2; np indicates not present.

in field photos (Figure 2). Based on this information, the saltmarsh habitats were classified into one of the following 5 vegetation cover classes: saltmarsh (SM), seagrass (SG), mangrove forest (MF), non-mangrove (terrestrial vegetation) forest (NMF), and agricultural land (AL) and 3 non-vegetated classes: saltpan (SP), wet sand (WS) and built-up areas (BA) to represent SM habitats and functional groups across the L2-wetland ecosystem.

Each of the aforementioned 8 LCTs was geolocated using a handheld GPS, with a positional accuracy of 3 m–4 m which is adequate for the satellite data of medium resolution with 30 m spatial resolution. Visual inspection of the high-resolution Google Earth map enabled us to choose target sampling locations prior to the GPS survey. The pixel-based point data on the location of each cover class were collected using GPS. A total of 1,729 GPS data were collected from the 3 study sites: L1 (457), L2 (866), and L3 (406) (Table 3). The GPS points were collected as close as possible from the transition of 2 classes to acquire more ground information for discriminating SM habitat types. For example, data were collected mainly from the borderline patches of SMs for separating SMs from WS areas. Some points were opportunistically taken from sites with SM dominated areas. The sample pixels selected as described above were randomly divided into the training set and the validation set, 932 and 797 sample pixels for training and validation set (Table 3) corresponding to the field-survey GPS points of 8 LCTs for the 3 sites (specifically 110, 150, 160, 131, 120, 115, 131 of training and 105, 109, 130, 129, 89, 93 of validation sample for SM, MF, NMF, AL, SP, and WS, respectively). 31 SG sample pixels were randomly divided into training (15) and a validation set (16) for L2. As the spatial distribution of SG was the smallest, field GPS data set for both training and validation among LCTs were the lowest, occupying the smallest area of the L2 wetland area.

Landsat 8 data: image selection, acquisition and pre-processing

The orthorectified and Level 1 terrain corrected (L1T) Landsat 8 Operational Land Imager (OLI) data of Worldwide Reference System (WRS2), processed by the L1 Product Generation System (LPGS) and provided by the United States Geological Survey (USGS); <http://earthexplorer.usgs.gov>) were used in this study. The single tile path 136 row 45 acquired on December 28, 2017 was used for mapping the locations L1 and L2 (Figure 1). Additionally, path 135 row 46 acquired on January 17, 2016 was used in mapping the land-cover types in the location L3 and their surrounding SM habitats. Both images were acquired at approximately 12:20 UTC at low tide to allow the maximum extent of mudflat to be observable and to minimize light attenuation effects caused by high-tides (Hossain et al. 2015, 2016). Tide data were taken from the web interface established by Oregon State University (WorldTides; <https://www.worldtides.info>) 4 pixel locations ($20^{\circ}44'52.05''$ N, $92^{\circ}19'25.99''$ E; $21^{\circ}6'28.9''$ N, $91^{\circ}55'12.27''$ E; $22^{\circ}6'31.26''$ N, $91^{\circ}50'37.92''$ E; $22^{\circ}13'19.08''$ N, $91^{\circ}47'51.32''$ E) were randomly selected to determine tide-heights. Note, field data and coincident cloud-free and low tide Landsat acquisition was impossible for studying the external validation site L3. Considering the high tide height of wetland areas around L3 and common cloudiness which limit the right acquisition of Landsat images, field data collected in June–July 2016 were used to analyze the scene acquired on January 17, 2016 and compromised with seasonal differences that may have between these dates. However, the effects of seasonal variations on the predictive performance of classifiers would not be an issue as this study did not use multitemporal Landsat imagery, rather, the same set of training and validation sets were used for the analysis of a single image with a view to test the performance of classifiers.

Table 4. Bands and spectral wavelengths of Landsat 8 OLI used in this study.

Band	Spectrum	Wavelength Range (nm)	Centre Wavelength (nm)	Bandwidth (nm)
B1	Aerosol	435–451	443	16
B2	Blue	452–512	482	60.1
B3	Green	533–590	561.5	57.4
B4	Red	636–673	654.5	37.5
B5	NIR	851–879	865	28.2
B6	SWIR-1	1,566–1,651	1608.5	84.7
B7	SWIR-2	2,107–2,294	2200.5	186.7

The OLI data have $30\text{ m} \times 30\text{ m}$ spatial resolutions over a 12-bit dynamic range. For image processing, the OLI bands 1–7 were selected in this study. The spectral characteristics of the bands is presented in Table 4. The spectral and spatial information about OLI are available elsewhere (Irons et al. 2012).

The raw digital numbers of the image were converted to radiance in order to perform radiometric correction and these radiance values were further converted to at surface reflectance (atmospheric correction) using the FLAASH (Fast Line-of-Sight Atmospheric Analysis of the Spectral Hypercube) module in ENVI 5.3 (Matthew et al. 2002). Following the radiometric and atmospheric corrections, the subset images were created from the satellite scene to facilitate data analysis only within the LCT areas of the SM (Figure 3).

Saltmarsh LCT mapping methodology

Each saltmarsh LCT was extracted by a rule-based classification approach, consisting of a specific classification scheme for discriminating certain features. Both already established image processing techniques and newly developed set of cascade rules based on structured in a hierarchical tree (image thresholding from spectral indices) were applied on the satellite images. Figure 3 shows the rule sets and image classification processes developed for the saltmarsh LCT mapping, in which spectral indices were selected from pre-established indices, and some new indices are proposed.

Land-water separation

Prior to the classification, the intertidal mudflats, SM vegetation, and wetland areas were isolated from surrounding surface water pixels (step-1 in Figure 3) using a mask developed from an optimal NIR threshold value (Mondejar and Tongco 2019; Hossain et al. 2015).

SG and BA classifications

In step-2, SG and BA were identified from the land-masked image (Figure 3). SG and BA were classified

using preestablished “seed pixel growing technique on the enhanced image” (M.S. Hossain et al. 2016; Hossain et al. 2015) and conventional Normalized Difference Built-up Index (NDBI) respectively (Table 5) in the image used for mapping L2 (Figure 3). To implement image enhancement technique, the true color image (bands 4, 3, and 2) was manually enhanced through adjusting brightness, contrast, and sharpness such that seagrass meadow (which is exposed during low tide) is displayed as gray to give the surrounding substrates maximum contrast (Hossain et al. 2015). The visual interpretation of the enhanced image helped in recognizing the boundary of seagrass meadows. Next, seed pixel growing technique (Adams and Bischof 1994; Pratt 2007) was applied to the enhanced image, where training data collected over seagrass meadows were used as seed for the implementation of this process (Hossain et al. 2016). Since SG was only found in L2 this step was skipped while analyzing images for L1 and L3. A threshold of zero, with positive values BA, along with or without SG (depends on the availability of SG-cover class) masked images were isolated and retained for further processing.

Spectral index development

Spectral analysis of SG and BA-masked images revealed that multispectral bands may not be adequate for extracting the information required for remaining LCT classifications. Spectral characteristics of LCTs in terms of multispectral information (OLI B1–B7) over L2 were analyzed (Figure 4). Analysis of spectral signatures showed that the identification could be accomplished with manipulation of indices with the main contribution from the less utilized SWIR-1 and 2 bands. Both SM and WS spectra are extremely close to SP. The spectral trends in Figure 4 illustrate how difficult it is in attempting to discriminate these LCTs. Reflectance spectra in bands B5–B7 clearly show that there is, in fact, obvious spectral confusion between WS and SM. There is a sharp increase in reflectance for NMF and MF between bands 4 and 5 is much greater than for AL, while SM, WS, and SP remain low in reflectance in that spectral range. The existence

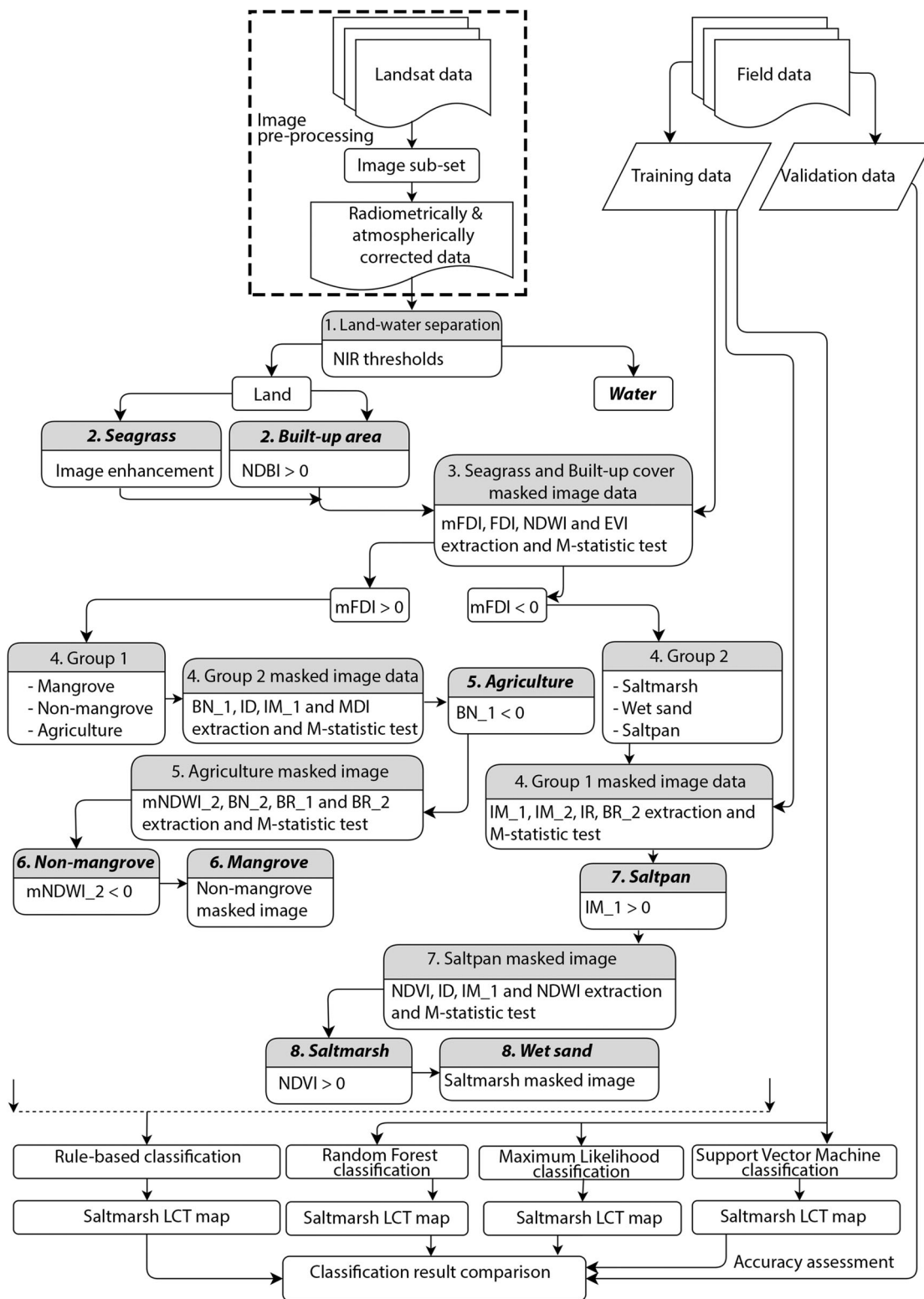


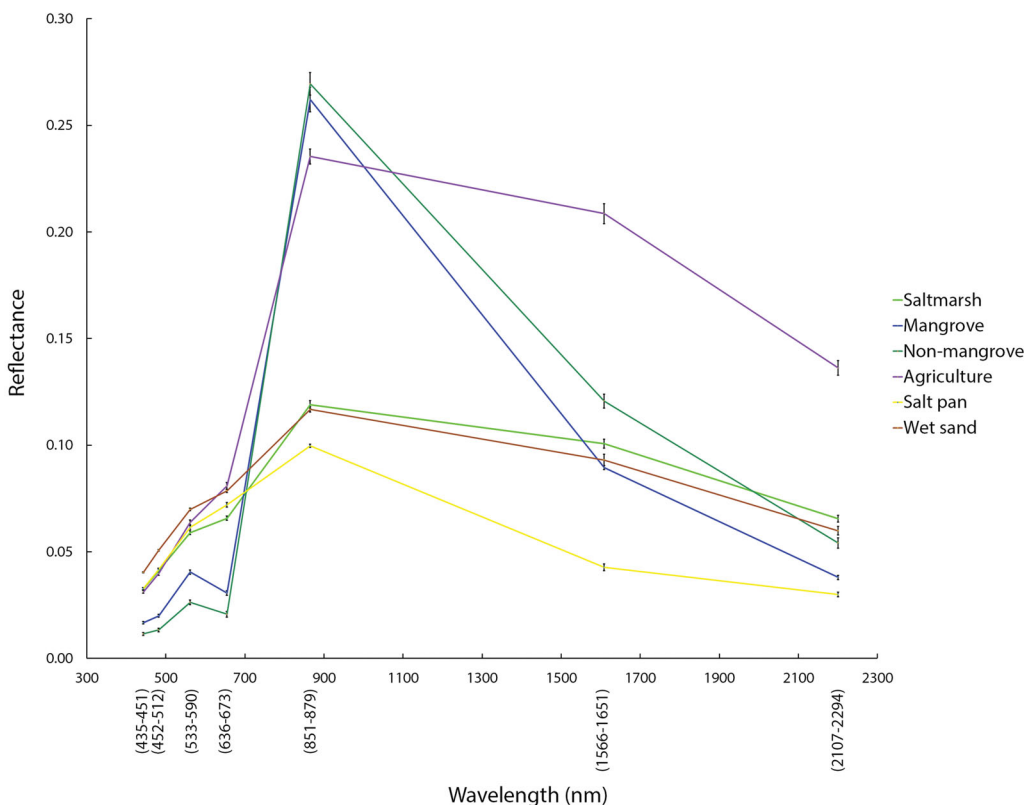
Figure 3. Flowchart of the proposed rule-based classification method for saltmarsh land-cover type (LCT) classification over the Bakkhali estuary (L2). Steps followed in conducting the classification of LCTs are numbered sequentially.

of wet mudflat within MF and NMF in the wetland areas sharply declines from B5 to B6 at a higher rate compared to SP. Bands B6 and B7 can be chosen to separate AL because only AL is more reflective in

those wavelengths. However, using a single band or choosing the right combination of bands would be a challenge in order to discriminate such a spectrally confusing LCTs.

Table 5. Indices used in this study.

	Index	Formula	Reference
Vegetation indices	Normalized Difference Vegetation Index (NDVI)	$\frac{(B5-B4)}{(B5+B4)}$	(Tucker 1979)
	Forest Discrimination Index (FDI)	$B5 - (B3 + B4)$	(Kamal et al. 2015)
	Modified Forest Discrimination Index (mFDI)	$B5 - (B2 + B3 + B4)$	modified from (Kamal et al. 2015)
	Enhanced Vegetation Index (EVI)	$\frac{2.5 \times (B5-B4)}{(B5+2.4 \times B4+1)}$	(Ghosh et al. 2016)
Water indices	Mangrove Discrimination Index (MDI)	$\frac{(B5-B7)}{B7}$	(Wang et al. 2020)
	Normalized Difference Water Index (NDWI)	$\frac{(B3-B5)}{(B3+B5)}$	(Gao 1996)
	Modified Normalized Difference Water Index _{SWIR-1} (mNDWI_1)	$\frac{(B3-B6)}{(B3+B6)}$	(Xu 2006)
Band ratio	Modified Normalized Difference Water Index _{SWIR-2} (mNDWI_2)	$\frac{(B3-B7)}{(B3+B7)}$	Modified from (Xu 2006)
	SWIR-1-to-Coastal Blue ratio (BR_1)	$\frac{B6}{B1}$	This study
Normalized spectral index	SWIR-2-to-Coastal Blue ratio (BR_2)	$\frac{B7}{B1}$	This study
	Band normalization-1 (BN_1)	$\frac{(B3-B4)}{(B3+B4)}$	This study
	Band normalization-2 (BN_2)	$\frac{(B7-B1)}{(B7+B1)}$	This study
Index difference	Index difference (ID)	$NDVI - NDWI$	This study
Index multiplication	Index multiplication-1 (IM_1)	$mNDWI_1 \times BR_1$	This study
Index ratio	Index multiplication-2 (IM_2)	$mNDWI_1 \times BR_2$	This study
	Index ratio (IR)	$\frac{mNDWI_2}{mNDWI_1}$	This study
Built-up index	Normalized Difference Built-up Index (NDBI)	$\frac{(B5-B4)}{\sqrt{(B5+B6)10}}$	(As-Syakur et al. 2012)

**Figure 4.** Spectral characteristics of target class-of-interest based on training data set, demonstrating more than 1 band is essential for discriminating them. Wavelength range values for each band of Landsat 8 OLI are given within parentheses.

In step-3, 4 widely used vegetation indices, 2 water-related spectral indices, and 1 impervious surface-related index were calculated from the atmospherically corrected (described earlier) OLI data: Normalized Difference Vegetation Index (NDVI) (Tucker 1979), Forest Discrimination Index (FDI) (Kamal et al. 2015), Enhanced Vegetation Index (EVI)

(Ghosh et al. 2016), Mangrove Discrimination Index (MDI) (Wang et al. 2018), Normalized Difference Water Index (NDWI) (Gao 1996), Modified Normalized Difference Water Index_{SWIR-1} (mNDWI_1) (Xu 2006) and Normalized Difference Built-up Index (NDBI) (As-Syakur et al. 2012) (step-3 in Figure 3).

This study has also used newly developed or modifier from previously developed one vegetation index, one water-related index, two band ratios, two normalized spectral indices, one index derived from the difference between index, and two indices derived from the multiplication of two indices: Modified Forest Discrimination Index (mFDI), Modified Normalized Difference Water Index SWIR-2 (mNDWI_2), SWIR-1-to-Coastal Blue ratio (BR_1), SWIR-2-to-Coastal Blue ratio (BR_2), Band normalization-1 (BN_1), Band normalization-2 (BN_2), Index difference (ID), Index multiplication-1 (IM_1)

Index multiplication-2 (IM_2) and Index ratio (IR). Details of the conventional, preestablished indices and the new derived indices used in this study are given in Table 5.

Saltmarsh LCT separability assessment

The classification scheme mainly consists of (i) grouping classes based on similarity of index value range, (ii) computing *M*-statistic for selecting the best index to be used for classification, (iii) apply index threshold for separating LCT. For the implementation of the threshold selection process, that allows a group of classes or specific LCT based on only binary splits, that is, a threshold of either positive or negative values of indices for each classification tree. The choice of the best option in terms of index manipulation was based on *M*-statistic for separating between group or individual LCT. The finally identified LCT was masked to easily identify remaining class without further involving the index threshold selection technique.

After the computation of the spectral indices, the separability between group or individual LCT test was performed using the *M*-statistics (Kaufman and Remer 1994) involving spectral indices. *M*-statistics is used as a separability estimator (Zhang and Tian 2013), based on the normalized mean distance, which assesses the separability between 2 classes through the amount of nonoverlapping they show. The *M*-statistic tests the separation between the histograms produced by plotting the frequency of all the pixel (index) values within 2 classes and the amount of separation between the histograms is defined by:

$$M = \frac{|\mu_1 - \mu_2|}{\sigma_1 + \sigma_2} \quad (1)$$

where μ_1 and μ_2 are average values for target classes 1 and 2, σ_1 and σ_2 are standard deviations for target classes 1 and 2. *M* values less than 1 indicate that classes significantly overlap and poor separability, while good separable classes are characterized by *M* values higher than one; higher the *M* value better is

the spectral characteristics or indices. *M*-statistic were calculated for each pair of indices in the region of interest (ROI), and 4 higher *M*-statistic were then compared for selecting the best suitable index for each of the LCT (Figure 3).

As highlighted in step-4 in Figure 3, LCTs were grouped into 2 preliminary target classes: (i) SM, SP and WS, and (ii) MF, NMF, and AL. The idea of a grouping of these LCTs emerged from plots of error bar graphs (Figure 5) generated from the standard deviation of the mean over ROI, where overlaps indicate the similarity of LCTs and criteria of LCT to be in the same group. Of the 4 indices, including mFDI, FDI, NDWI, and EVI, (Figure 5a-d) index with the highest *M*-statistic, that is, mFDI was used for grouping these classes. *M*-statistic value was also used for choosing BN_1, mNDWI_2, IM_1 and NDVI as the best index (Figure 5e-h) respectively for separating the following group/individual LCT: (i) AL from MF + NMF (step-5 in Figure 3), (ii) NMF from MF (step-6 in Figure 3), (iii) SP from SM + WS (step-7 in Figure 3) and (iv) SM from WS (step-8 in Figure 3), respectively (Table 6).

MF, NMF, and AL classifications. Error-bar graph also guided to limit a threshold for LCT discrimination at every stage of classification split. The choice of an index, with a threshold limit, were defined using the same criteria of *M*-statistic. AL areas were identified using the BN_1 index and a threshold of negative values (Figure 5e). Positive values of this index had NMF and MF LCTs. To separate MF from NMF, mNDWI index was used, with a threshold of negative values for NMF (Figure 5f). The NMF masked image indicated areas covered with only MF (Figure 3).

SM, WS, and SP classifications. The threshold that allowed the separation of the SM was mFDI < 0 (Figure 3 and Table 6). Negative values of the selected index indicated SM and other LCTs (WS and SP) with a similar spectral response. Thus, a complementary step was necessary to extract the SM alone. This was performed computing the IM_1 (see Table 5 for formula), where positive values of this index were identified as SP (Figures 3 and 5 g). Finally, SMs were identified extracting positive values of NDVI (Figure 5h) from SP masked image (Figure 3).

Performance of rule-based classification test

Furthermore, to test the relative performance of the rule-based classification scheme implemented using the index threshold, the results of three other commonly followed supervised algorithms were compared,

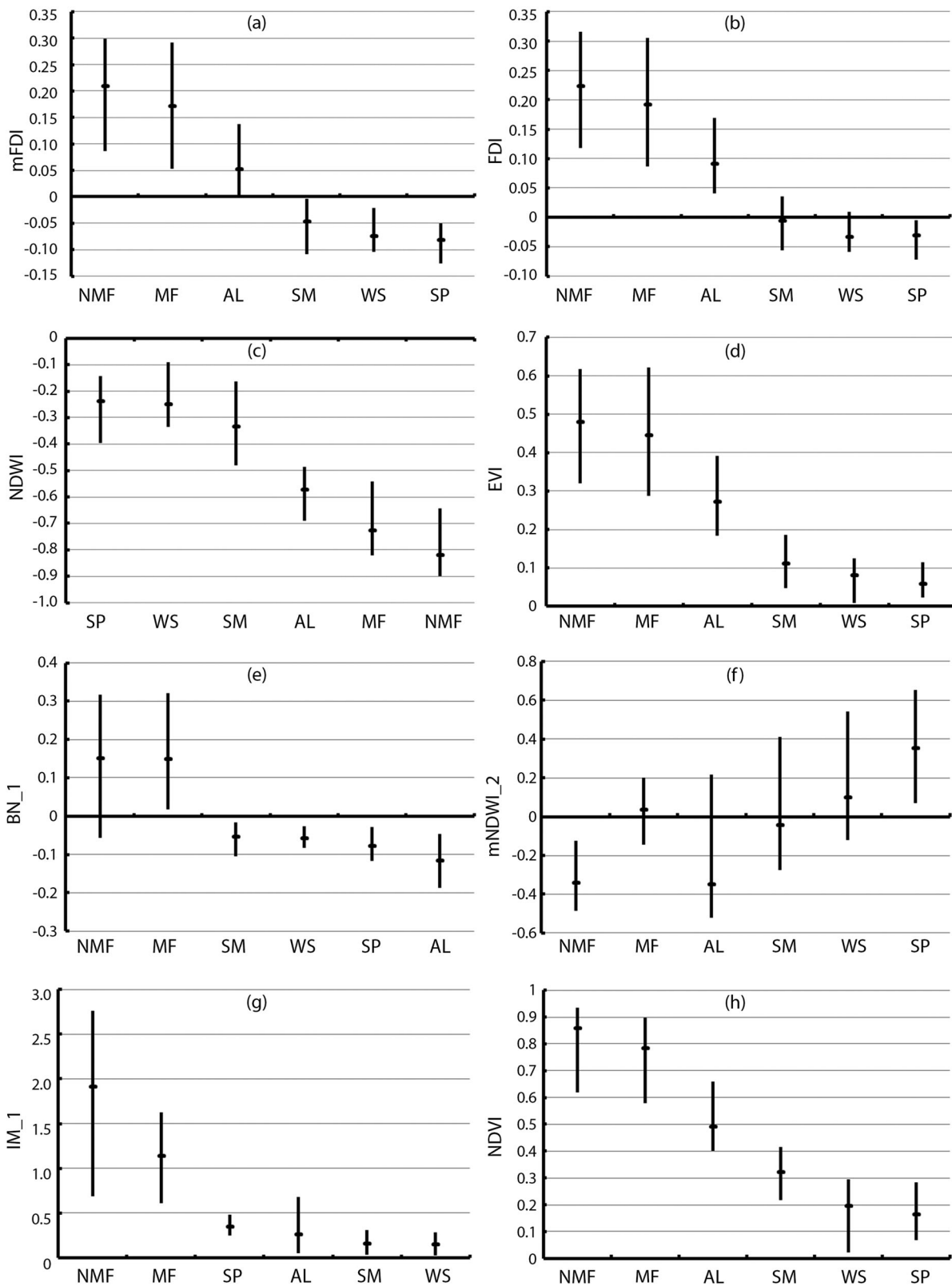


Figure 5. Comparison of spectral responses (nodes represent the mean values and error bars represent the standard deviation of indices): (a) mFDI, (b) FDI, (c) NDWI, (d) EVI, (e) BN_1, (f) mNDWI_2, (g) IM_1, and (h) NDVI to 6 different saltmarsh land-cover types (LCT), over the classification scheme development site L2. The LCT and index abbreviations are as in Tables 1 and 3 respectively.

Table 6. The *M*-statistic values between saltmarsh land-cover types (LCTs).

Saltmarsh LCT		Index	<i>M</i> -statistic
Class 1	Class 2		
AL	MF + NMF	mFDI	2.261
		FDI	2.159
		NDWI	2.086
		EVI	1.969
		BN_1	2.304
		ID	2.016
NMF	MF	IM_1	1.713
		MDI	1.650
		mNDWI_2	2.426
		BN_2	2.032
		BR_2	1.983
SP	SM + WS	BR_1	1.938
		IM_1	2.480
		IM_2	2.355
		IR	1.246
		BR_2	1.230
SM	WS	NDVI	2.776
		ID	2.756
		IM_1	1.740
		NDWI	1.728

Finally selected spectral index for discriminating LCT is in bold. The LCT and index abbreviations are as in [Tables 2](#) and [5](#), respectively.

namely: Random Forest (RF), Maximum Likelihood classifier (MLC), and Support Vector Machines (SVM). 17 different spectral features (indices in [Table 5](#)) generated to implement rule-based classification scheme and the same training data ([Table 3](#)) sampled over 8 cover classes ([Table 2](#)) were tested as input for RF, MLC, and SVM classifications ([Figure 3](#)). It is important to note that training data used for developing feature layers for L2 for rule-based classification were no longer used for classifying external validation sites L1 and L3. The optimum spectral indices revealed from L2 site analysis and their thresholds were used for L1 and L3 instead. The site-specific training data given in [Table 3](#) were used for running the rest of the test classifiers, that is, RF, SVM, and MLC.

The RF classifier is a non-parametric, ensemble decision tree-based algorithm developed in the field of machine learning (Breiman 2001) and is robust to variations in class reflectance caused by heterogeneous landscapes (Timm and McGarigal 2012; Khatami et al. 2016). The RF classifications were performed in EnMAP (Environmental Mapping and Analysis Program), a freely available toolbox developed at the Humboldt University (Berlin), useful for the processing of spectral imagery (Van der Linden et al. 2015). This toolbox has many built-in classification algorithms, including the RF module.

Like RF, SVM is another machine learning classifier. When MLC is based on canonical, conditional class distribution and Bayesian inference (Richards and Jia 2006), SVM is based on sequential minimal

optimization for training and adopts a linear kernel (Keerthi et al. 2001). The MLC uses the means and variances of the training data to estimate the probability of class membership belonging to a pixel and pixel is assigned in a class with a maximum probability of membership. The SVM with the radial basis function (Hsu et al. 2010; Kavzoglu and Colkesen 2009) and the MLC classifications were performed in ENVI 5.3. The focus of this study was not to search for optimum parameters so as to improve the accuracy of RF, MLC, or SVM results. Hence, the default values were used during the implementation of these classifiers for the scope of the work.

Accuracy assessment

The accuracy of classification results was calculated using overall classification accuracy (OA) (using independent field data set reserved for validation purposes; [Figure 3](#) and [Table 3](#)), Kappa (K) statistics, User's Accuracy (UA) and Producer's Accuracy (Jensen 2004; Cohen 1960) for all the 3 sites (L1, 2 and 3).

Results

Comparison of spectral indexes based on *M*-statistic test

[Table 6](#) shows the LCT groups and spectral index selection processes developed for the Bakhali wetland (L2), in which some spectral indices are selected and combined (mNDWI_1 and BR_1 or BR_2 as explained in [Table 5](#)), and some new spectral indices are proposed (BR_1, BR_2, ID, IM_1, IM_2, and IR as explained in [Table 5](#)). All indices were extracted from Landsat 8 remote sensing images over L2. The *M*-statistic values between LCTs which were further calculated by employing the training data sets of each LCT class. The *M*-statistic test results indicated potential indices (11 indices given in [Table 5](#)) which had the ability to separate the LCT classification categories.

In order to increase *M*-statistic values, this study introduced band B2 (all visible bands were included) in formulating mFDI ([Table 5](#)), which is a little modification of FDI. Although NDWI and EVI were widely used to detect surface water and non-water bodies respectively, this study found mFDI (with *M*-statistic = 2.26; [Table 6](#)) is the best for separating between target categories (between Groups 1 and 2 in [Figure 3](#)) being *M*-statistic maximum. However, there were no significant differences between mFDI (2.26) and FDI (2.16) in terms of *M*-statistic score for L2 ([Table 6](#)). Also, the threshold of all positive values of both

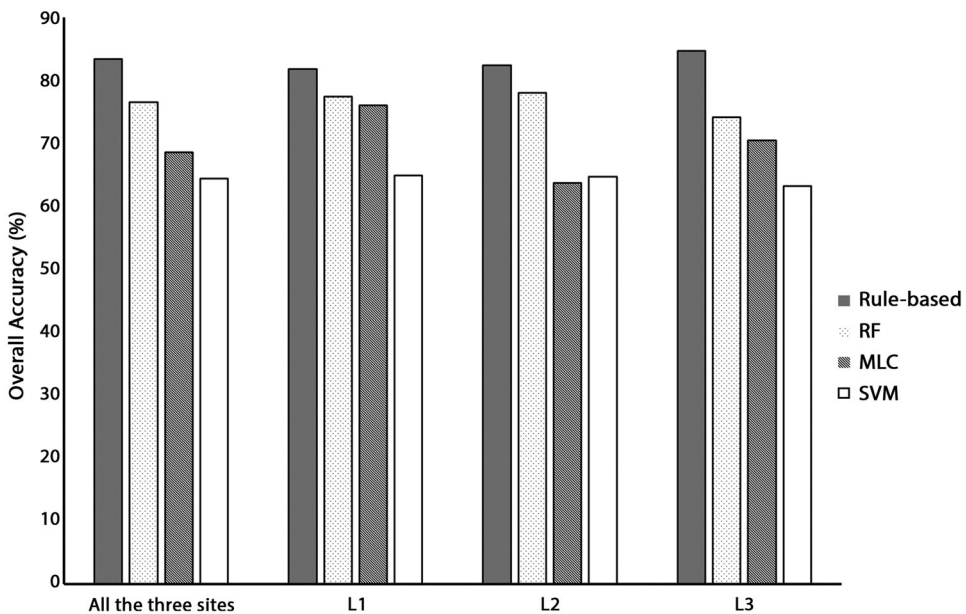


Figure 6. Overall accuracy achieved by rule-based, RF, MLC, and SVM classifiers for saltmarsh LCT mapping for individual sites (L1, L2, and L3) and all the 3 sites.

indices can be used for detecting Group 1 (Figure 5a). Therefore, $FDI > 0$ can be used as a supplementary criterion to separate Group 1 from Group 2 pixels. NDWI can only differentiate Group 1 from Group 2 with the ability similar to that of FDI (2.09) but cannot identify SM from WS (1.73). Among the M -statistic values, only M -statistic of BN_1 and IM_1 showed the greatest ability to discriminate AL and SP respectively from other target LCTs (Table 6).

A general increase in group or individual LCT class separability is observed when using normalization of 2 bands, with respect to using the best multiplication between index (IM_1) or using previously established MDI, with a rise from 1.65 to 1.71 for AL (worst) separability, and from 2.03 (for NMF using BN_2) to 2.30 (for AL using BN_1; best separability) for L2 wetland system.

If the spectral normalization commonly used for water detection is employed, NDWI with the modified form suggested in this study, the separability between MF and NMF can be improved. For example, using mNDWI_2, the M -statistic can be achieved as 2.43. However, the most commonly used vegetation index NDVI can also contribute to separate SM from the spectrally confusing WS class (Figure 5h), with the goodness of separability 2.78. Optionally, the difference between NDVI and NDWI (represents ID) can be used in separating them (Table 6). ID can also distinguish AL from MF + NMF, with M -statistic = 2.02. Thus, some indices found useful in discriminating more than 1 LCT features. IM_1 can slightly distinguish AL from MF + NMF and SM from WS, while it

can effectively discriminate SP from SM + WS. This is the only index that appeared in most of the times (3 times) in the top 4 potential spectral indices.

Based on the above analysis, for separating between LCT, a single index does not effectively discriminate 1 LCT from the other target LCTs. Consequently, by selecting the best index (see bold texts in Table 6), the ability to distinguish SM from other vegetation as well as non-vegetation cover types in the whole classification can be enhanced.

Performance of saltmarsh LCT classification

Saltmarsh covers classification tests were performed using the rule-based vegetation index selection approach, combining all three test sites (L1–L3; Figure 6 and Table 7). Validation dataset independent from the training dataset calculated a satisfactory classification with an OA of 83.3% for the rule-based classifier. Accuracy assessment results achieved using a rule-based classification approach was compared with 3 other supervised classification algorithms, using the same spectral feature layer and training input dataset. The overall accuracies of the rule-based LCTs classification were considerably higher than those for RF, MLC and SVM (8.5%, 19.5%, and 25.7%, respectively). The overall accuracy of SVM was consistently the smallest for all study sites (L1–L3) (Figure 6). All tested classifiers achieved lower accuracy performance compared to the proposed rule-based approach for test site L2, with the best result reached with rule-based classification ($OA = 84.6\%$, $K = 0.821$), followed

Table 7. User and producer accuracies of saltmarsh LCT maps created using the rule-based, RF, MLC and SVM classification techniques applied to the method development test site L2 (Bakkhali river estuary) and the two external validation test sites L1 (Karnaphuli river estuary) and L3 (Teknaf peninsula).

	Method	Rule-based	RF	MLC	SVM
All sites	<i>K</i>	0.81	0.73	0.64	0.59
UA (PA)	SM	76 (92)	79 (65)	53 (49)	53 (52)
	SG	93 (81)	75 (56)	33 (69)	50 (50)
	MF	74 (91)	75 (74)	82 (64)	69 (60)
	NMF	78 (75)	74 (68)	80 (73)	73 (63)
	AL	91 (79)	76 (85)	73 (81)	68 (83)
	SP	86 (78)	75 (80)	63 (83)	53 (72)
	WS	84 (76)	69 (77)	66 (55)	71 (68)
	BA	97 (92)	89 (90)	72 (71)	66 (55)
L1	<i>K</i>	0.79	0.73	0.72	0.59
	UA (PA)	SM	96 (92)	88 (54)	88 (58)
	SG	np	np	np	np
	MF	50 (100)	63 (88)	81 (88)	62 (72)
	NMF	73 (31)	85 (63)	82 (66)	53 (51)
	AL	94 (85)	79 (95)	80 (90)	83 (73)
	SP	100 (92)	66 (84)	52 (88)	46 (76)
	WS	81 (100)	82 (64)	88 (100)	73 (86)
L2	<i>K</i>	0.80	0.75	0.58	0.57
	UA (PA)	SM	83 (90)	77 (60)	58 (30)
	SG	93 (81)	75 (56)	33 (69)	50 (50)
	MF	83 (89)	82 (78)	94 (54)	64 (52)
	NMF	75 (89)	79 (83)	76 (94)	77 (78)
	AL	90 (68)	80 (78)	64 (73)	64 (87)
	SP	84 (76)	89 (74)	58 (74)	56 (71)
	WS	80 (82)	58 (82)	38 (32)	64 (64)
L3	<i>K</i>	0.82	0.70	0.61	0.58
	UA (PA)	SM	50 (100)	78 (95)	37 (95)
	SG	np	np	np	np
	MF	100 (87)	77 (57)	70 (63)	90 (63)
	NMF	85 (93)	50 (43)	100 (37)	100 (43)
	AL	89 (96)	66 (88)	85 (88)	64 (88)
	SP	77 (67)	71 (83)	82 (90)	58 (70)
	WS	100 (48)	85 (81)	100 (56)	84 (59)
	BA	97 (90)	96 (81)	74 (74)	76 (42)

The LCT abbreviations are as in Table 2.

K: Kappa coefficient of agreement; UA: user's accuracy; PA: producer's accuracy; np: not present in the site.

by RF (OA = 78%, $K=0.745$), MLC (OA = 63.6%, $K=0.582$), and SVM (OA = 64.7%, $K=0.59$) (Table 7 and Figure 6).

The spectral index thresholding scheme was applied to the SM occurring areas in the Bakkhali estuary (L2) for producing LCT maps for coastal and inland wetland areas (Figure 7). The proposed approach was tested in 2 validation sites for generating LCT maps for each wetland area (L1 and L3; Figures 8 and 9, respectively).

NMF are found dominating in the inland areas (Figure 9a). The dominance of BA was observed in the southern tip of L3 (Figure 8d). L1 areas were dominated by AL and NMF, while L3 areas were dominated by NMF and BA, with sparse SM sporadically present along the shorelines in both the locations. Of the 8 LCTs, SG occupied the smallest area by 0.01% of the entire wetland L2 (Figure 7), while it was absent in other 2 sites L1 and L3. SM had the highest coverage with 10.4% of the total wetland L2 and the

lowest over L1 (0.8%). WS occupied the smallest area by 0.8% and 0.6% of the wetlands L1 and L3 respectively. In the rule-based classification map of the three major vegetated LCTs, NMF was the most extensive cover type that occupied 75.1% and 29.4% of the wetland areas L3 and L1, while AL was the largest coverage with 42.1% in L1 (Figures 8 and 9).

Both visual assessment and quantitative examination of classification results and produced maps (Figures 7–9) revealed that the spectral features of WS were similar to SM class. However, since spectral characteristics were considerably different due to vegetated and non-vegetated LCT, image masking and index threshold selection approach largely corrected this confusion, which improved the PA for SM for all the 3 sites to 75% compared to 65%, 49%, and 52% with RF, MLC, and SVM, respectively (Table 7).

Discussion

The general perception is that saltmarshes are flat open areas (Eiser and Kjerfve 1986). They are large stands of homogeneous vegetation types (Hunter and Power 2002) or exist within the intertidal zone where varieties of halophytic plants form the marsh platform (Hladik and Alber 2012). However, saltmarshes do not occur alone; mangrove, saltmarsh, and terrestrial vegetation coexist in many wetlands in the world (Saintilan et al. 2019). A typical coastal saltmarsh ecosystem comprises terrestrial vegetation dominated by large forest trees and shrubs which is rarely inundated by coastal waters. Next to this zone, saltmarsh can occur in 3 different water regimes: areas that experience water stagnancy for occasional, short-term, and throughout the year (Wilcox 2002). Such information is important for mapping landscape patterns and wetland vegetation distribution. However, depending on project objectives and required details of wetland cover classification, medium resolution remote sensing imagery like Landsat OLI data may be too coarse for accurate discrimination of the spectrally similar LCTs in heterogeneous saltmarsh areas (Pham et al. 2019).

The prediction of SM distribution from high-resolution images (i.e., WorldView-2 and QuickBird) using RF was found to be superior to traditional classifiers (Ouyang et al. 2011; Timm and McGarigal 2012). The accuracy results achieved in this study also revealed that RF was superior to MLC and SVM, however, it failed to outperform rule-based classifier when applied to Landsat. The classification error rate of RF is related to inter-tree correlation; the greater the correlation, the greater the error. Optimum selection of variables for the setting of RF classification

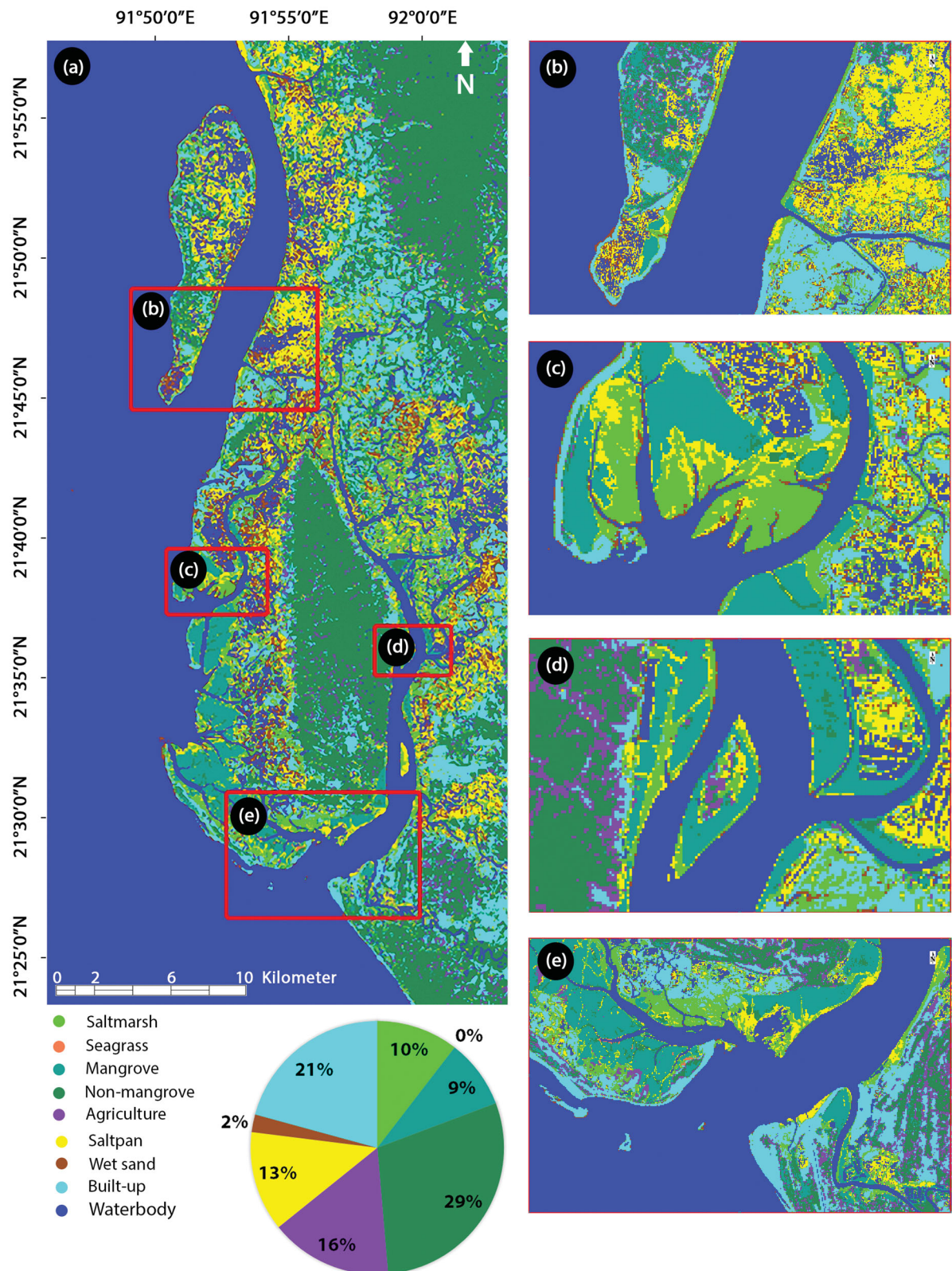


Figure 7. Saltmarsh land-cover type maps generated using the proposed rule-based approach for the method development site, the Bakkhali estuary (L2). (a) illustrates the overall view, and (b–e) zoomed-in views for some of the saltmarsh abundant regions. The class abbreviations are as in Table 2.

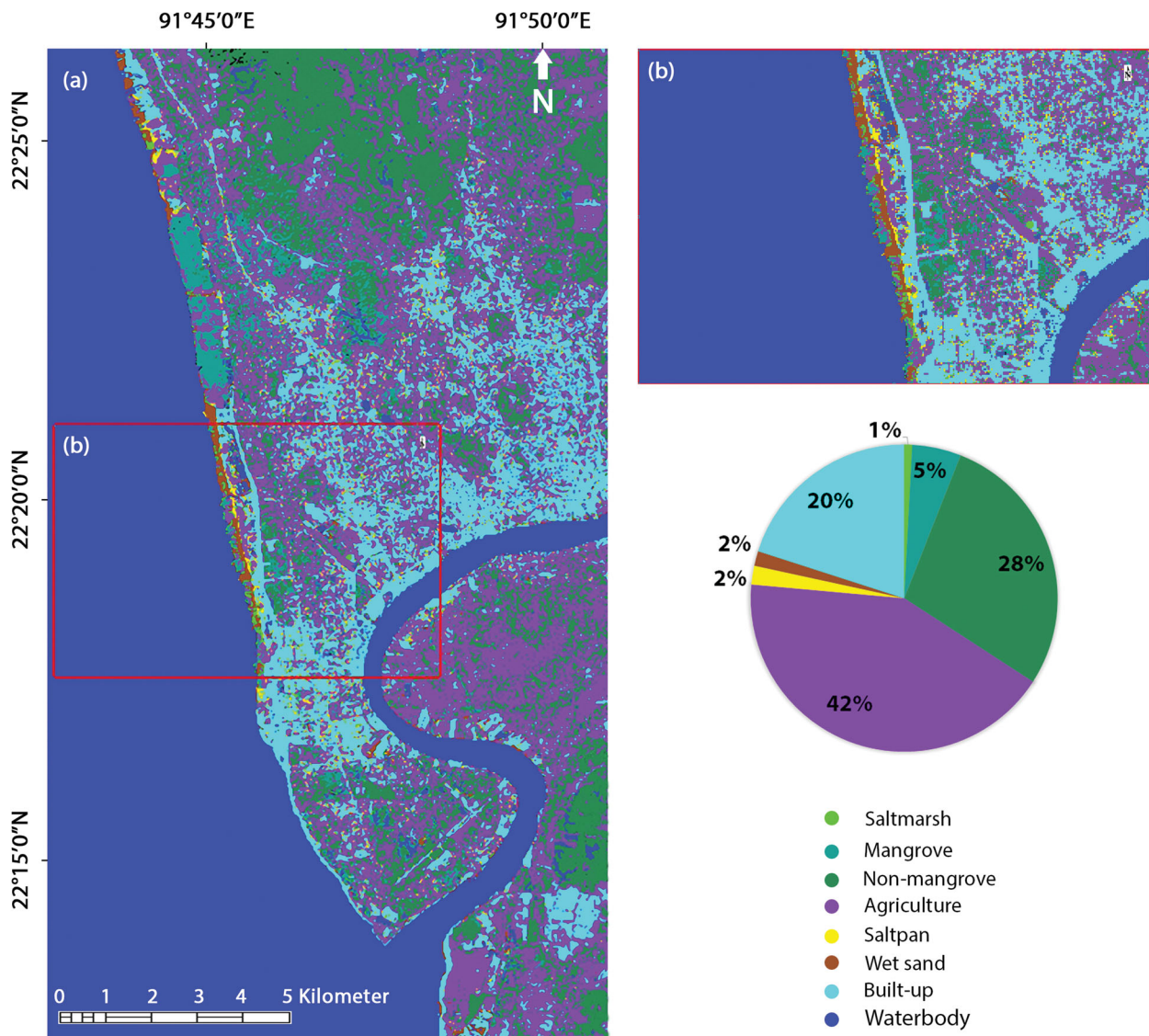


Figure 8. Saltmarsh land-cover type maps generated using the proposed rule-based approach for the external validation site, the Karnaphuli river estuary (L1). (a) illustrates the overall view, and (b) zoomed-in view of the saltmarsh abundant region. The class abbreviations are as in Table 2.

may improve its classification accuracy (Speiser et al. 2019). The spectral similarity between spectral similar LCTs could be one of the possible reasons behind failing to achieve higher accuracy than that of the rule-based classifier. Results presented in the previous section demonstrate the feasibility and reliability of designing a hierarchical decision rule based on index thresholds (Figure 3) applied to Landsat OLI at 30 m spatial resolution for mapping 5 vegetation cover classes (SM, SG, MF, NMF, AL) distinctly from other non-vegetated cover classes (WS and SP) in south-western Bangladesh (Figures 7–9). A combination of simple and robust algorithms and open-sourced OLI data-enabled LCT mapping with higher classification accuracy ($OA > 80\%$), compared to other supervised classification methods (RF, MLC, and SVM) (Figure 6 and Table 7).

More than 1 index or combined indices showed almost equally efficient in terms of spectral separability (referred to M -statistic) to discriminate between LCTs (Tables 5 and 6). Therefore, the user has flexibility in choosing spectral index depending on site characteristics and the method can additionally be modified in order to detect target class(es) of interest. Such results also support the use of index thresholding and masking approach not only for distinguishing MF from NMF, as others have previously demonstrated (Gupta et al. 2018; Zhang and Tian 2013) but also for enhancing the capabilities of multispectral remote sensing to classify SM use and cover types, which would be difficult to discriminate using traditional vegetation index (for example, NDVI threshold alone is not always workable) or commonly used

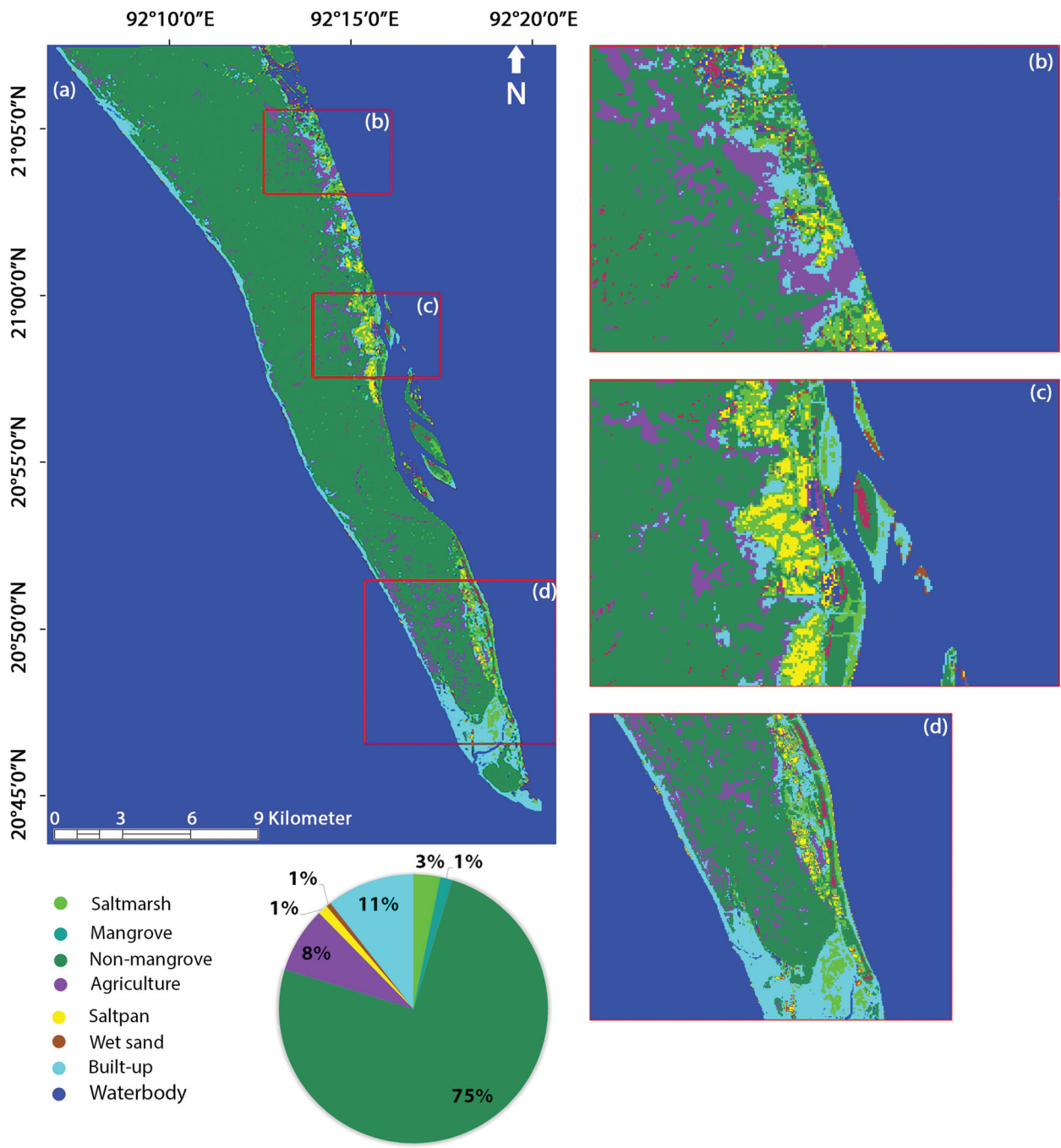


Figure 9. Saltmarsh land-cover type maps generated using the proposed rule-based approach for the external validation site, the Teknaf Peninsula (L3). (a) illustrates the overall view, and (b-d) zoomed-in views for some of the saltmarsh abundant regions. The class abbreviations are as in Table 2.

classifiers (MLC, SVM, etc.) only. Other studies have also shown that commonly used vegetation and water indices have not been very effective in discriminating vegetation species in wetland environments (Gupta et al. 2018; Zhang et al. 2011).

The proposed method has demonstrated the ability to differentiate between NMF and SM which is rarely found in published researches. This is very important if we want to assess changes in SM habitats and to understand the pattern, direction, and magnitude of

changes. Therefore, SM loss if caused by land-use changes can be detected using this approach (Figure 3).

Landsat time-series have widely been used for SM vegetation analysis due to their long historical archive and free-available datasets, covering almost all over the coasts of the world (Pham et al. 2019). Previous studies that have mapped SM vegetation based on a monthly NDVI time-series analysis from Landsat acquisition that has generally observed that season is

one of the important factors for facilitating the discrimination of the SM communities (Sun et al. 2018). Some have demonstrated the potential use of light detection and ranging (LIDAR) technologies to classify SM vegetation based on edaphic variables, such as elevation (Hladik and Alber 2012; Yeo et al. 2020), salinity, moisture and water table (Hladik and Alber 2014) in explaining vertical zonation of SM. These studies have used a variety of remote sensing data and methods, including classification and regression trees (CART), linear discrimination analysis (LDA), canonical correspondence analysis (CCA). Tidal creek characteristics in saltmarshes were extracted from LIDAR, based on elevation and slope thresholds (Chirol et al. 2018). Although all these studies considered edaphic and topographic variables to understand SM ecosystem processes, where SM was considered as a single LCT and none tested a combination of multiple methods for discriminating both vegetated and non-vegetated target classes of interest within SM ecosystem.

However, mapping was affected by the impure nature of pixels caused by mixed vegetations. There were areas with SM but with WS in the background (Figure 2c). Similarly, there were areas with MF but with either SM or WS in the background. The open canopy of SM vegetation allowed the WS to contribute significantly to the spectral signature from the background. There was a substantial amount of water both in WS and SP so they were difficult to separate from each other. Moreover, there were many small water-clogged areas and ponds within the SM vegetation. In such water codominant areas, differentiation between SM and WS or SP was difficult due to the dominance of water reflectance. The near-infrared band was attenuated by the occurrence of background water, WS, and SP (Kumar and Sinha 2014; Hestir et al. 2008; Zomer et al. 2009). Thus, classification accuracies were also affected by the amount of water as a background. Once SM, WS, and SP were grouped together, some indices with high *M*-statistic showed the ability to separate them from the group comprising of MF, NMF, and AL. However, this shows the difficulty in separating SM from other LCTs, especially in the areas where water dominating feathers, such as SP and WS co-exist.

The accuracy of the rule-based classification scheme is partly affected by the moderate resolution of Landsat OLI. The inaccuracies of OLI in LCT discrimination can be attributed to 30 m spatial resolution. This resolution may not be adequate to capture narrow (sparsely distributed vegetation) CTs because there are similar biochemical and biophysical

properties in the wetland ecosystems. Besides the background effects, the size of SM and WS is also critical for accurate retrieval of spectral signatures. As the areal coverage of SM and WS patches are often smaller than the size of a single Landsat pixel (i.e., less than 90 m²), mixed pixel problem arises and consequently, the similarity of spectral information of these 2 classes can propagate to as the classification error. The previous studies suggested that high spatial resolution imagery can provide adequate details of spectral properties of saltmarsh species in a fragmented patch (Rasel et al. 2016).

The spectral variations within LCTs can also be due to vegetation, soil and water background, and micro-climatic conditions, and local stressors (Adam et al. 2010). The optical properties of multispectral reflectance are affected by these factors and the sensor commonly informs us lower reflectance, especially in the near-infrared and shortwave infrared regions (B5–B7 in OLI; Table 3) where water attenuation is high (Silva et al. 2008). Nevertheless, the results of this research have demonstrated that multispectral imagery can be used to separate SM wetlands from non-SM vegetated and unvegetated areas. Refining the spectral index threshold for the end-member selection criteria through analysis of multitemporal Landsat data may potentially improve the spectral separability between these 2 classes; however, alternative image classification techniques should also be investigated. The recently launched (on June 23, 2015) Sentinel-2 is considered to be follow-up mission to the Landsat, intended to maintain remote sensing data supply continuity (Malenovský et al. 2012). Compared to Landsat OLI, Senstinel-2 has a better spatial (with a resolution of 10 m–60 m) and better spectral resolution in the NIR region and 3 Red Edge regions (with a resolution of 20 m). Combining data from additional sensors, such as Sentinel-2, may improve the ability to discriminate spectrally similar SM and WS (Darvishzadeh et al. 2019).

The proposed rule-based approach reduced background noise which introduced spectral confusion in previous efforts and suggested hyperspectral remote sensing in previous studies. However, the feasibility and robustness of this rule-based approach are limited to some factors: (*i*) the band(s) of remote sensors used to extract indices. The index formulation involves coastal, visible, near-infrared, and short-wave infrared bands, which may not match with other sensors and consequently, may make the implementation of the rule-based approach impossible. (*ii*) The tidal dynamics which may introduce large uncertainty. This

study only used Landsat images acquired during the low tides within the study sites so that more subtidal SM and tidal flat areas could be identified, and the effects of tidal dynamics would be negligible. The quality (cloud and shadow-free images) and temporal instability of input Landsat images at both temporal and spatial scales have posed significant challenges to LCT mapping (Wang et al. 2020; Gong et al. 2013).

For conservation and management of coastal ecosystems require detailed baseline information on the distribution and coverage of the wetland resources, as well as the ability to perform retrospective remote sensing for monitoring the changes in SM ecosystems. The results of the study can be used as baseline information for understanding SM habitat loss and change in land use and cover. For example, Sun et al. (2018) used NDVI extracted from multitemporal Landsat imagery for classification of SM communities, showed a tremendous loss of upper SM, and conversion of SM area to other land-uses with acceptable accuracies (OA = 0.898). Though this study and other reports (Sun et al. 2016; Eastwood et al. 1997; Laengner et al. 2019) have classified SM communities in the study area relatively homogeneous, there is a need to establish baseline data for heterogeneous and dynamic wetland ecosystem at suitable wetland scale for long-term monitoring. The proposed rule-based approach and the results have achieved this task. However, there is immense scope of further researches to improve the classification accuracy and can be extended in subsequent researches. (i) To improve the class separability (M -statistic) between vegetated LCTs, satellite imagery acquired in a suitable period of growing season of the species of interest can be used as inputs prior to vegetation index manipulation (Sun et al. 2018; Villa et al. 2015; Wang et al. 2012; Sinha et al. 2012a). (ii) Since there is the possibility of increasing accuracy through involving a combination of different spectral indices (Table 5), good results could be achieved choosing proper time-series remote sensing data where spatial and temporal resolution, along with knowledge about variations in the phenology of species with temporal variability is essential for species/community differentiation (Sinha et al. 2012b). Locals and ecologists may help informing about the best suitable time of the year when the species present have optimal discrimination. (iii) Further study may establish relationships between edaphic variables including leaf and canopy characteristics and remote sensing variables including spectral indices as some have observed biophysical parameters as a good indicator in discriminating SM and other coastal vegetations (Hladik and Alber 2014; Zheng et al. 2016; Kamal et al. 2016). (iv) Another

prospective research to improve classification accuracy is through comparing the performance of more advanced image classification techniques such as Artificial or multibranch convolutional neural network (MBCNN), CART, etc, and some have reported benefits of using these techniques in coastal vegetation classification (Wang et al. 2020; Becker et al. 2007; Zhang and Tian 2013; Feng et al. 2019).

Conclusion

A wise decision on image data and algorithms are 2 of several influential factors that may make mapping efforts successful and improve mapping accuracy. Our results clearly show that the rule-based classification approach applied for generating saltmarsh LCT maps at 30-m spatial resolution of Landsat imagery at the estuary scale is possible. The single index is not useful to reveal all LCTs of SM. In this study, the Landsat-based vegetation indices, water-related indices, ratio indices, and manipulation of indices captured the LCT including coastal vegetation, mudflats, and impervious surfaces with training datasets in enough detail and achieved adequate accuracy. Improvements in the discrimination of wetland vegetation can be made if multitemporal imagery and ancillary information such as elevation, slope, or bathymetry are incorporated in the classification scheme. Further research is required to derive a good spectral index of wetland vegetation from free available images with higher spatial and temporal resolutions (e.g., Sentinel-1 and 2), which could be an alternative to costly hyperspectral data and hopefully will further improve coastal wetland mapping in the future.

The LCT maps of coastal Bangladesh are likely to provide vital information for ecological, geographical applications, and economic implications. The produced map holds important environmental information: the location and extent of small isolated SM and zones of SM vegetation are of relevance to conservation, as is the coverage of intertidal WS used as feeding ground for shorebirds, SP used for economic activities of coastal people, and BA is an indicator of anthropogenic disturbance on coastal resources and all these information help coastal zone management and developing a sustainable plan.

ACKNOWLEDGMENTS

Landsat 8 OLI data were downloaded from the USGS Earthexplorer portal (<http://earthexplorer.usgs.gov>). For having assisted in saltmarsh land-cover type field data collection the authors thank Arannayk Foundation—Wetland conservation campaigns.

Disclosure statement

No potential conflict of interest was reported by the author(s).

Funding

This work was financially supported by the National Agricultural Technology Program—Phase II, Bangladesh Agricultural Research Council (BARC), Bangladesh; the Higher Institution Centre of Excellence (HICoE) Research Grant [53209], awarded to the Institute of Oceanography and Environment (INOS), Universiti Malaysia Terengganu (UMT); Arannayk Foundation—Wetland conservation campaigns [AF-Saltmarsh-15070101].

ORCID

Sheikh Mohammed Rabiul Alam  <http://orcid.org/0000-0002-3419-4769>

Mohammad Shawkat Hossain  <http://orcid.org/0000-0002-1974-7169>

References

- Abu Hena, M.K., Aysha, A., Ashraful, M.A.K.K., Sharifuzzaman, S.M., Akhtar, A., Ashraful, M.A.K.K., and Sharifuzzaman, S.M. 2010. "Distribution of aquatic macrophytes in the coastal area of Salimpur, Chittagong, Bangladesh." *Chiang Mai University Journal of Natural Sciences*, Vol. 9(No. 2): pp. 273–279.
- Adam, E., Mutanga, O., and Rugege, D. 2010. "Multispectral and hyperspectral remote sensing for identification and mapping of wetland vegetation." *Wetlands Ecology and Management*, Vol. 18(No. 3): pp. 281–296. doi:[10.1007/s11273-009-9169-z](https://doi.org/10.1007/s11273-009-9169-z).
- Adams, R., and Bischof, L. 1994. "Seeded region growing." *IEEE Transactions on Pattern Analysis and Machine Intelligence*, Vol. 16(No. 6): pp. 641–647. doi:[10.1109/34.295913](https://doi.org/10.1109/34.295913).
- Alam, M.W., and Zafar, M. 2013. "Occurrences of *Salmonella* spp. in water and soil sample of the Karnaphuli River estuary." *Microbes and Health*, Vol. 1(No. 2): pp. 41–45. doi:[10.3329/mh.v1i2.14087](https://doi.org/10.3329/mh.v1i2.14087).
- As-Syakur, A.R., Adnyana, I.W.S., Wayan Arthana, I., and Wayan Nuarsa, I. 2012. "Enhanced Built-Up and Bareness Index (EBBI) for mapping built-up and bare land in an urban area." *Remote Sensing*, Vol. 4(No. 10): pp. 2957–2970. doi:[10.3390/rs4102957](https://doi.org/10.3390/rs4102957).
- Becker, B.L., Lusch, D.P., and Qi, J. 2007. "A classification-based assessment of the optimal spectral and spatial resolutions for great lakes coastal wetland imagery." *Remote Sensing of Environment*, Vol. 108(No. 1): pp. 111–120. doi:[10.1016/j.rse.2006.11.005](https://doi.org/10.1016/j.rse.2006.11.005).
- Belluco, E., Camuffo, M., Ferrari, S., Modenese, L., Silvestri, S., Marani, A., and Marani, M. 2006. "Mapping salt-marsh vegetation by multispectral and hyperspectral remote sensing." *Remote Sensing of Environment*, Vol. 105(No. 1): pp. 54–67. doi:[10.1016/j.rse.2006.06.006](https://doi.org/10.1016/j.rse.2006.06.006).
- Breiman, L. 2001. "Random Forests." *Machine Learning*, Vol. 45(No. 1): pp. 5–32. doi:[10.1023/A:1010933404324](https://doi.org/10.1023/A:1010933404324).
- Chirol, C., Haigh, I.D., Pontee, N., Thompson, C.E., and Gallop, S.L. 2018. "Parametrizing tidal creek morphology in mature saltmarshes using semi-automated extraction from LiDAR." *Remote Sensing of Environment*, Vol. 209: pp. 291–311. doi:[10.1016/j.rse.2017.11.012](https://doi.org/10.1016/j.rse.2017.11.012).
- Chowdhury, M., Sh, N., S Hossain, M., Mitra, A., and Barua, P. 2011. "Environmental functions of the Teknaf Peninsula mangroves of Bangladesh to communicate the values of goods and services." *Mesopotamian Journal of Marine Science*, Vol. 26(No. 1): pp. 79–97.
- Civco, D., Hurd, J., Prisloe, S., and Gilmore, M. 2006. "Characterization of Coastal Wetland Systems Using Multiple Remote Sensing Data Types and Analytical Techniques." Paper presented at IEEE International Conference on Conference of Geoscience and Remote Sensing Symposium (IGRASS), Denver, CO, July 31–August 4, 2006.
- Cohen, J. 1960. "A coefficient of agreement for nominal scales." *Educational and Psychological Measurement*, Vol. 20(No. 1): pp. 37–46. doi:[10.1177/00131644600200104](https://doi.org/10.1177/00131644600200104).
- Costanza, R., d'Arge, R., de Groot, R., Farber, S., Grasso, M., Hannon, B., Limburg, K., et al. 1997. "The value of the world's ecosystem services and natural capital." *Nature*, Vol. 387(No. 6630): pp. 253–260. doi:[10.1038/387253a0](https://doi.org/10.1038/387253a0).
- Crooks, S., Tamelander, J., Laffoley, D., and March, J. V. 2011. *Mitigating climate change through restoration and management of coastal wetlands and near-shore marine ecosystems: Challenges and opportunities*. Washington, DC: World Bank.
- Darvishzadeh, R., Wang, T., Skidmore, A., Vrieling, A., O'Connor, B., Gara, T., Ens, B., and Paganini, M. 2019. "Analysis of Sentinel-2 and RapidEye for retrieval of leaf area index in a saltmarsh using a radiative transfer model." *Remote Sensing*, Vol. 11(No. 6): pp. 671. doi:[10.3390/rs11060671](https://doi.org/10.3390/rs11060671).
- Das, B., Khan, Y.S.A., and Sarker, M.A.K. 2002. "Trace metal concentration in water of the Karnaphuli River Estuary of the Bay of Bengal." *Pakistan Journal of Biological Sciences*, Vol. 5(No. 5): pp. 607–608. doi:[10.3923/pjbs.2002.607.608](https://doi.org/10.3923/pjbs.2002.607.608).
- Davy, A. J. 2000. "Development and structure of salt marshes: Community patterns in time and space BT - Concepts and controversies in tidal marsh ecology." In *Concepts and Controversies in Tidal Marsh Ecology*, edited by M.P. Weinstein and D.A. Kreeger, 137–156. Dordrecht, The Netherlands: Springer.
- Department of Environment. 2015. "Community based ecosystem conservation and adaptation in ecologically critical areas of Bangladesh: Responding to nature and changing climate." <https://portals.iucn.org/library/sites/library/files/documents/2015-053.pdf>
- Duarte, C.M., Dennison, W.C., Orth, R.J.W., and Carruthers, T.J.B. 2008. "The charisma of coastal ecosystems: Addressing the imbalance." *Estuaries and Coasts*, Vol. 31(No. 2): pp. 233–238. doi:[10.1007/s12237-008-9038-7](https://doi.org/10.1007/s12237-008-9038-7).
- Eastwood, J.A., Yates, M.G., Thomson, A.G., and Fuller, R.M. 1997. "The reliability of vegetation indices for monitoring saltmarsh vegetation cover." *International Journal*

- of *Remote Sensing*, Vol. 18(No. 18): pp. 3901–3907. doi: [10.1080/014311697216739](https://doi.org/10.1080/014311697216739).
- Eiser, W.C., and Kjerfve, B. 1986. "Marsh topography and hypsometric characteristics of a South Carolina salt marsh basin." *Estuarine, Coastal and Shelf Science*, Vol. 23(No. 5): pp. 595–605. doi:[https://doi.org/10.1016/0272-7714\(86\)90101-0](https://doi.org/10.1016/0272-7714(86)90101-0). doi: [10.1016/0272-7714\(86\)90101-0](https://doi.org/10.1016/0272-7714(86)90101-0).
- Feng, Q., Yang, J., Zhu, D., Liu, J., Guo, H., Bayartungalag, B., and Li, B. 2019. "Integrating multitemporal sentinel-1/2 data for coastal land cover classification using a multi-branch convolutional neural network: A case of the Yellow River Delta." *Remote Sensing*, Vol. 11(No. 9): pp. 1006. doi: [10.3390/rs09](https://doi.org/10.3390/rs09).
- Gallant, L.A. 2015. "The challenges of remote monitoring of wetlands." *Remote Sensing*, Vol. 7(No. 8): pp. 10938–10950. doi: [10.3390/rs08](https://doi.org/10.3390/rs08).
- Gao, B.-c. 1996. "NDWI—A normalized difference water index for remote sensing of vegetation liquid water from space." *Remote Sensing of Environment*, Vol. 58(No. 3): pp. 257–266. doi: [10.1016/S0034-4257\(96\)00067-3](https://doi.org/10.1016/S0034-4257(96)00067-3).
- Gedan, K.B., Silliman, B.R., and Bertness, M.D. 2009. "Centuries of human-driven change in salt marsh ecosystems." *Annual Review of Marine Science*, Vol. 1(No. 1): pp. 117–141. doi: [10.1146/annurev.marine.010908.163930](https://doi.org/10.1146/annurev.marine.010908.163930).
- Ghosh, S., Mishra, D.R., and Gitelson, A.A. 2016. "Long-term monitoring of biophysical characteristics of tidal wetlands in the Northern Gulf of Mexico - A methodological approach using MODIS." *Remote Sensing of Environment*, Vol. 173: pp. 39–58. doi: [10.1016/j.rse.2015.11.015](https://doi.org/10.1016/j.rse.2015.11.015).
- Gong, P., Wang, J., Yu, L., Zhao, Y., Zhao, Y., Liang, L., Niu, Z., et al. 2013. "Finer resolution observation and monitoring of global land cover: First mapping results with Landsat TM and ETM + data." *International Journal of Remote Sensing*, Vol. 34(No. 7): pp. 2607–2654. doi: [10.1080/01431161.2012.748992](https://doi.org/10.1080/01431161.2012.748992).
- Gupta, K., Mukhopadhyay, A., Giri, S., Chanda, A., Datta Majumdar, S., Samanta, S., Mitra, D., Samal, R.N., Pattnaik, A.K., and Hazra, S. 2018. "An index for discrimination of mangroves from non-mangroves using LANDSAT 8 OLI imagery." *MethodsX*, Vol. 5: pp. 1129–1139. doi: [10.1016/j.mex.2018.09.011](https://doi.org/10.1016/j.mex.2018.09.011).
- Harvey, K.R., and Hill, G.J.E. 2001. "Vegetation mapping of a tropical freshwater swamp in the northern territory, Australia: A comparison of aerial photography, Landsat TM and SPOT satellite imagery." *International Journal of Remote Sensing*, Vol. 22(No. 15): pp. 2911–2925. doi: [10.1080/01431160119174](https://doi.org/10.1080/01431160119174).
- Hestir, E.L., Khanna, S., Andrew, M.E., Santos, M.J., Viers, J.H., Greenberg, J.A., Rajapakse, S.S., and Ustin, S.L. 2008. "Identification of invasive vegetation using hyperspectral remote sensing in the California Delta ecosystem." *Remote Sensing of Environment*, Vol. 112(No. 11): pp. 4034–4047. doi: [10.1016/j.rse.2008.01.022](https://doi.org/10.1016/j.rse.2008.01.022).
- Hladik, C., and Alber, M. 2012. "Accuracy assessment and correction of a LIDAR-Derived Salt Marsh Digital Elevation Model." *Remote Sensing of Environment*, Vol. 121: pp. 224–235. doi: [10.1016/j.rse.2012.01.018](https://doi.org/10.1016/j.rse.2012.01.018).
- Hladik, C., and Alber, M. 2014. "Classification of salt marsh vegetation using edaphic and remote sensing-derived variables." *Estuarine, Coastal and Shelf Science*, Vol. 141: pp. 47–57. doi: [10.1016/j.ecss.2014.01.011](https://doi.org/10.1016/j.ecss.2014.01.011).
- Hossain, M.S. 2001. "Biological aspects of the coastal and marine environment of Bangladesh." *Ocean & Coastal Management*, Vol. 44(No. 3–4): pp. 261–282. doi: [10.1016/S0964-5691\(01\)00049-7](https://doi.org/10.1016/S0964-5691(01)00049-7).
- Hossain, M.S., Bujang, J.S., Zakaria, M.H., and Hashim, M. 2015. "Application of Landsat images to seagrass areal cover change analysis for Lawas, Terengganu and Kelantan of Malaysia." *Continental Shelf Research*, Vol. 110: pp. 124–148. doi: [10.1016/j.csr.2015.10.009](https://doi.org/10.1016/j.csr.2015.10.009).
- Hossain, M.S., Bujang, J.S., Zakaria, M.H., and Hashim, M. 2016. "Marine and human habitat mapping for the coral triangle initiative region of Sabah using Landsat and Google Earth imagery." *Marine Policy*, Vol. 72: pp. 176–191. doi: [10.1016/j.marpol.2016.07.003](https://doi.org/10.1016/j.marpol.2016.07.003).
- Hsu, C. C., Chang, C. C., and Lin, C. J. 2010. *A practical guide to support vector classification*. Taipei, Taiwan: National Taiwan University.
- Hunter, E.L., and Power, C.H. 2002. "An assessment of two classification methods for mapping Thames Estuary intertidal habitats using CASI Data." *International Journal of Remote Sensing*, Vol. 23(No. 15): pp. 2989–3008. (Taylor & Francis: doi: [10.1080/01431160110075596](https://doi.org/10.1080/01431160110075596)).
- Hunter, P.D., Gilvear, D.J., Tyler, A.N., Willby, N.J., and Kelly, A. 2010. "Mapping macrophytic vegetation in shallow lakes using the compact airborne spectrographic imager (CASI)." *Aquatic Conservation: Marine and Freshwater Ecosystems*, Vol. 20(No. 7): pp. 717–727. doi: [10.1002/aqc.1144](https://doi.org/10.1002/aqc.1144).
- Irons, J.R., Dwyer, J.L., and Barsi, J.A. 2012. "The next Landsat Satellite: The Landsat data continuity mission." *Remote Sensing of Environment*, Vol. 122: pp. 11–21. doi: [10.1016/j.rse.2011.08.026](https://doi.org/10.1016/j.rse.2011.08.026).
- Jafar, S., Mollah, A. R., and Rahman, M. 2013. "Conservation of marine turtles in some coastal areas of Bangladesh and implications for the development of a national policy regime." In *30th Annual Symposium on Sea Turtle Biology and Conservation*, edited by A. F. Rees, Janice Blumenthal, A. Panagopoulou. Goa, India: International Sea Turtle Society (ISTS).
- Jensen, J. R. 2004. *Introductory digital image processing*. 3rd ed. New Jersey: Prentice Hall.
- Joshi, N., Baumann, M., Ehamer, A., Fensholt, R., Grogan, K., Hostert, P., Jepsen, M., et al. 2016. "A review of the application of optical and radar remote sensing data fusion to land use mapping and monitoring." *Remote Sensing*, Vol. 8(No. 1): pp. 70. doi: [10.3390/rs08010070](https://doi.org/10.3390/rs08010070).
- Kamal, M., Phinn, S., and Johansen, K. 2015. "Object-based approach for multi-scale mangrove composition mapping using multi-resolution image datasets." *Remote Sensing*, Vol. 7(No. 4): pp. 4753–4783. doi: [10.3390/rs07040](https://doi.org/10.3390/rs07040).
- Kamal, M., Phinn, S., and Johansen, K. 2016. "Assessment of multi-resolution image data for mangrove leaf area index mapping." *Remote Sensing of Environment*, Vol. 176: pp. 242–254. doi: [10.1016/j.rse.2016.02.013](https://doi.org/10.1016/j.rse.2016.02.013).
- Kangas, P.C., and Lugo, A.E. 1990. "The distribution of mangroves and saltmarsh in Florida." *Tropical Ecology*, Vol. 31(No. 1): pp. 32–39.
- Kantakumar, L.N., and Neelamsetti, P. 2015. "Multi-temporal land use classification using hybrid approach." *The*

- Egyptian Journal of Remote Sensing and Space Science*, Vol. 18(No. 2): pp. 289–295. doi:[10.1016/j.ejrs.2015.09.003](https://doi.org/10.1016/j.ejrs.2015.09.003).
- Kaufman, Y.J., and Remer, L.A. 1994. “Detection of forests using mid-IR reflectance: An application for aerosol studies.” *IEEE Transactions on Geoscience and Remote Sensing*, Vol. 32(No. 3): pp. 672–683. doi:[10.1109/36.297984](https://doi.org/10.1109/36.297984).
- Kavzoglu, T., and Colkesen, I. 2009. “A kernel functions analysis for support vector machines for land cover classification.” *International Journal of Applied Earth Observation and Geoinformation*, Vol. 11(No. 5): pp. 352–359. doi:[10.1016/j.jag.2009.06.002](https://doi.org/10.1016/j.jag.2009.06.002).
- Keerthi, S.S., Shevade, S.K., Bhattacharyya, C., and Murthy, K.R.K. 2001. “Improvements to Platt’s SMO algorithm for SVM classifier design.” *Neural Computation*, Vol. 13(No. 3): pp. 637–649. doi:[10.1162/089976601300014493](https://doi.org/10.1162/089976601300014493).
- Khatami, R., Mountrakis, G., and Stehman, S.V. 2016. “A meta-analysis of remote sensing research on supervised pixel-based land-cover image classification processes: General guidelines for practitioners and future research.” *Remote Sensing of Environment*, Vol. 177: pp. 89–100. doi:[10.1016/j.rse.2016.02.028](https://doi.org/10.1016/j.rse.2016.02.028).
- Klemas, V. 2013. “Remote sensing of emergent and submerged wetlands: An overview.” *International Journal of Remote Sensing*, Vol. 34(No. 18): pp. 6286–6320. doi:[10.1080/01431161.2013.800656](https://doi.org/10.1080/01431161.2013.800656).
- Kulawardhana, R.W., Popescu, S.C., and Feagin, R.A. 2014. “Fusion of LiDAR and multispectral data to quantify salt marsh carbon stocks.” *Remote Sensing of Environment*, Vol. 154: pp. 345–357. doi:[10.1016/j.rse.2013.10.036](https://doi.org/10.1016/j.rse.2013.10.036).
- Kumar, L., and Sinha, P. 2014. “Mapping salt-marsh land-cover vegetation using high-spatial and hyperspectral satellite data to assist wetland inventory.” *GIScience & Remote Sensing*, Vol. 51(No. 5): pp. 483–497. (Taylor & Francis: doi:[10.1080/15481603.2014.947838](https://doi.org/10.1080/15481603.2014.947838).
- Laengner, L.M., Siteur, K., and van der Wal, D. 2019. “Trends in the seaward extent of saltmarshes across Europe from long-term satellite data.” *Remote Sensing*, Vol. 11(No. 14): pp. 1653. doi:[10.3390/rs14](https://doi.org/10.3390/rs14).
- Lara, R.J., Neogi, S.B., Islam, M.S., Mahmud, Z.H., Yamasaki, S., and Nair, G.B. 2009. “Influence of catastrophic climatic events and human waste on vibrio distribution in the Karnaphuli Estuary, Bangladesh.” *EcoHealth*, Vol. 6(No. 2): pp. 279–286. doi:[10.1007/s10393-009-0257-6](https://doi.org/10.1007/s10393-009-0257-6).
- Lee, Y.-K., Park, J.-W., Choi, J.-K., Oh, Y., and Won, J.-S. 2012. “Potential uses of TerraSAR-X for mapping herbaceous halophytes over salt marsh and tidal flats.” *Estuarine, Coastal and Shelf Science*, Vol. 115: pp. 366–376. doi:[10.1016/j.ecss.2012.10.003](https://doi.org/10.1016/j.ecss.2012.10.003).
- Lira, C., and Taborda, R. 2014. “Advances in applied remote sensing to coastal environments using free satellite imagery.” In *Remote sensing and modeling: Advances in coastal and marine resources*, edited by C.W. Finkl and C. Makowski, 77–102. Cham, Switzerland: Springer International Publishing.
- Lopes, C.L., Mendes, R., Caçador, I., and Dias, J.M. 2019. “Evaluation of long-term estuarine vegetation changes through Landsat imagery.” *The Science of the Total Environment*, Vol. 653: pp. 512–522. doi:[10.1016/j.scitotenv.2018.10.381](https://doi.org/10.1016/j.scitotenv.2018.10.381).
- Maghsoudi, Y., Collins, M.J., and Leckie, D. 2012. “Speckle reduction for the forest mapping analysis of multi-temporal Radarsat-1 images.” *International Journal of Remote Sensing*, Vol. 33(No. 5): pp. 1349–1359. doi:[10.1080/01431161.2011.568530](https://doi.org/10.1080/01431161.2011.568530).
- Malenovský, Z., Rott, H., Cihlar, J., Schaepman, M.E., García-Santos, G., Fernandes, R., and Berger, M. 2012. “Sentinels for science: Potential of Sentinel-1, -2, and -3 missions for scientific observations of ocean, cryosphere, and land.” *Remote Sensing of Environment*, Vol. 120: pp. 91–101. doi:[10.1016/j.rse.2011.09.026](https://doi.org/10.1016/j.rse.2011.09.026).
- Matthew, M. W., Adler-Golden, S. M., Berk, A., Felde, G., Anderson, G. P., Gorodetzky, D., Paswaters, S., and Shippert, M. 2002. “Atmospheric correction of spectral imagery: Evaluation of the FLAASH algorithm with AVIRIS data.” Paper presented at the Applied Imagery Pattern Recognition Workshop, Washington, DC, October 16–18, 2002.
- McCarthy, M.J., Merton, E.J., and Muller-Karger, F.E. 2015. “Improved coastal wetland mapping using very-high 2-meter spatial resolution imagery.” *International Journal of Applied Earth Observation and Geoinformation*, Vol. 40: pp. 11–18. doi:[10.1016/j.jag.2015.03.011](https://doi.org/10.1016/j.jag.2015.03.011).
- Mcowen, C.J., Weatherdon, L.V., Van Bochove, J.-W., Sullivan, E., Blyth, S., Zockler, C., Stanwell-Smith, D., et al. 2017. “A global map of saltmarshes.” *Biodiversity Data Journal*, Vol. 5: pp. e11764. doi:[10.3897/BDJ.5.e11764](https://doi.org/10.3897/BDJ.5.e11764).
- Mondejar, J.P., and Tongco, A.F. 2019. “Near infrared band of Landsat 8 as water index: A case study around Cordova and Lapu-Lapu City, Cebu, Philippines.” *Sustainable Environment Research*, Vol. 29(No. 1): pp. 16. doi:[10.1186/s42834-019-0016-5](https://doi.org/10.1186/s42834-019-0016-5).
- Murray, N.J., Phinn, S.R., DeWitt, M., Ferrari, R., Johnston, R., Lyons, M.B., Clinton, N., Thau, D., and Fuller, R.A. 2019. “The global distribution and trajectory of tidal flats.” *Nature*, Vol. 565(No. 7738): pp. 222–225. doi:[10.1038/s41586-018-0805-8](https://doi.org/10.1038/s41586-018-0805-8).
- Ouyang, Z.-T., Gao, Y., Xie, X., Guo, H.-Q., Zhang, T.-T., and Zhao, B. 2013. “Spectral discrimination of the invasive plant *Spartina alterniflora* at multiple phenological stages in a saltmarsh wetland.” *PLoS One*, Vol. 8(No. 6): pp. e67315. doi:[10.1371/journal.pone.0067315](https://doi.org/10.1371/journal.pone.0067315).
- Ouyang, Z.-T., Zhang, M.-Q., Xie, X., Shen, Q., Guo, H.-Q., and Zhao, B. 2011. “A comparison of pixel-based and object-oriented approaches to VHR imagery for mapping saltmarsh plants.” *Ecological Informatics*, Vol. 6(No. 2): pp. 136–146. doi:[10.1016/j.ecoinf.2011.01.002](https://doi.org/10.1016/j.ecoinf.2011.01.002).
- Pendleton, L., Donato, D.C., Murray, B.C., Crooks, S., Jenkins, W.A., Sifleet, S., Craft, C., et al. 2012. “Estimating Global “blue carbon” emissions from conversion and degradation of vegetated coastal ecosystems.” *PLoS One*, Vol. 7(No. 9): pp. e43542. doi:[10.1371/journal.pone.0043542](https://doi.org/10.1371/journal.pone.0043542).
- Pham, T.D., Xia, J., Ha, N.T., Bui, D.T., Le, N.N., and Tekeuchi, W. 2019. “A review of remote sensing approaches for monitoring blue carbon ecosystems: Mangroves, seagrasses and salt marshes during 2010–2018.” *Sensors*, Vol. 19 (No. 8): pp. 1933. doi:[10.3390/s19081933](https://doi.org/10.3390/s19081933).

- Phiri, D., and Morgenroth, J. 2017. "Developments in Landsat land cover classification methods: A review." *Remote Sensing*, Vol. 9: pp. 967. doi:[10.3390/rs9090967](https://doi.org/10.3390/rs9090967).
- Pratt, W.K. 2007. "Image enhancement." In *Digital Image Processing*, 4th ed., 247–305. Los Altos, CA: Wiley-Interscience.
- Rasel, S.M.M., Chang, H.C., Diti, I.J., Ralph, T., and Saintilan, N. 2016. "Comparative analysis of Worldview-2 and Landsat 8 for coastal saltmarsh mapping accuracy assessment." In *Sensing for Agriculture and Food Quality and Safety VIII*, edited by M.S. Kim, K. Chao, and B.A. Chin, 1–13. Bellingham, WA: SPIE.
- Rasel, S.M.M., Chang, H.-C., Ralph, T.J., Saintilan, N., and Diti, I.J. 2019. "Application of feature selection methods and machine learning algorithms for saltmarsh biomass estimation using Worldview-2 imagery." *Geocarto International*. Advance online publication. doi:[10.1080/10106049.2019.1624988](https://doi.org/10.1080/10106049.2019.1624988).
- Rashed-Un-Nabi, M., Abdulla, M.A.M., Hadayet, M.U., and Mustafa, M.G. 2011. "Temporal and spatial distribution of fish and shrimp assemblage in the Bakkhali River Estuary of Bangladesh in relation to some water quality parameters." *Marine Biology Research*, Vol. 7(No. 5): pp. 436–452. doi:[10.1080/17451000.2010.527988](https://doi.org/10.1080/17451000.2010.527988).
- Richards, J. A., and Jia, X. 2006. *Remote sensing digital image analysis: An introduction*. Berlin, Germany: Springer.
- Rizbi, S. 1971. *Bangladesh District Gazetteers, Chittagong Government of Bangladesh*. Dacca, Bangladesh: Service and General Administration Department.
- Roy, J., Datta, S., Kapuria, P., Guha, I., Banerji, R., Miah, M., Islam, R., et al. 2019. "Coastal ecosystems and changing economic activities: Challenges for sustainability transition." APN Science Bulletin (Asia Pacific Network for Global Change Research), Vol. 3: pp. 1–137.
- Saintilan, N., Rogers, K., and McKee, K.L. 2019. "The shifting saltmarsh-mangrove ecotone in Australasia and the Americas." In *Coastal Wetlands*, edited by G.M.E. Perillo, E. Wolanski, and D.R. Cahoon, 915–945. Amsterdam; Oxford, UK; Cambridge, US: Elsevier. doi:[10.1016/B978-0-444-63893-9.00026-5](https://doi.org/10.1016/B978-0-444-63893-9.00026-5).
- Sharifuzzaman, S. M. 1988. *A review of climatic condition of the coastal belt of Bangladesh*. Chittagong, Bangladesh: University of Chittagong.
- Silva, T.S.F., Costa, M.P.F., Melack, J.M., and Novo, E.M.L.M. 2008. "Remote sensing of aquatic vegetation: Theory and applications." *Environmental Monitoring and Assessment*, Vol. 140(No. 1–3): pp. 131–145. doi:[10.1007/s10661-007-9855-3](https://doi.org/10.1007/s10661-007-9855-3).
- Silvestri, S., Marani, M., and Marani, A. 2003. "Hyperspectral remote sensing of salt marsh vegetation, morphology and soil topography." *Physics and Chemistry of the Earth, Parts A/B/C*, Vol. 28(No. 1–3): pp. 15–25. doi:[https://doi.org/10.1016/S1474-7065\(03\)00004-4](https://doi.org/10.1016/S1474-7065(03)00004-4). doi:[10.1016/S1474-7065\(03\)00004-4](https://doi.org/10.1016/S1474-7065(03)00004-4).
- Sinha, P., Kumar, L., and Reid, N. 2012a. "Three-date Landsat thematic mapper composite in seasonal land-cover change identification in a mid-latitudinal region of diverse climate and land use." *Journal of Applied Remote Sensing*, Vol. 6(No. 1): pp. 063595. doi:[10.1117/1.JRS.6.063595](https://doi.org/10.1117/1.JRS.6.063595).
- Sinha, P., Kumar, L., and Reid, N. 2012b. "Seasonal variation in land-cover classification accuracy in a diverse region." *Photogrammetric Engineering & Remote Sensing*, Vol. 78(No. 3): pp. 271–280. doi:[10.14358/PERS.78.3.271](https://doi.org/10.14358/PERS.78.3.271).
- Speiser, J.L., Miller, M.E., Tooze, J., and Ip, E. 2019. "A comparison of random forest variable selection methods for classification prediction modeling." *Expert Systems with Applications*, Vol. 134: pp. 93–101. doi:[10.1016/j.eswa.2019.05.028](https://doi.org/10.1016/j.eswa.2019.05.028).
- Sun, C., Fagherazzi, S., and Liu, Y. 2018. "Classification mapping of salt marsh vegetation by flexible monthly NDVI time-series using landsat imagery." *Estuarine, Coastal and Shelf Science*, Vol. 213: pp. 61–80. doi:[10.1016/j.ecss.2018.08.007](https://doi.org/10.1016/j.ecss.2018.08.007).
- Sun, C., Liu, Y., Zhao, S., Zhou, M., Yang, Y., and Li, F. 2016. "Classification mapping and species identification of salt marshes based on a short-time interval NDVI time-series from HJ-1 optical imagery." *International Journal of Applied Earth Observation and Geoinformation*, Vol. 45: pp. 27–41. doi:[10.1016/j.jag.2015.10.008](https://doi.org/10.1016/j.jag.2015.10.008).
- Timm, B., and McGarigal, K. 2012. "Fine-scale remotely-sensed cover mapping of coastal dune and salt marsh ecosystems at Cape Cod National Seashore using random forests." *Remote Sensing of Environment*, Vol. 127: pp. 106–117. doi:[10.1016/j.rse.2012.08.033](https://doi.org/10.1016/j.rse.2012.08.033).
- Tucker, C.J. 1979. "Red and photographic infrared linear combinations for monitoring vegetation." *Remote Sensing of Environment*, Vol. 8(No. 2): pp. 127–150. doi:[https://doi.org/10.1016/0034-4257\(79\)90013-0](https://doi.org/10.1016/0034-4257(79)90013-0). doi:[10.1016/0034-4257\(79\)90013-0](https://doi.org/10.1016/0034-4257(79)90013-0).
- van Beijma, S., Comber, A., and Lamb, A. 2014. "Random forest classification of salt marsh vegetation habitats using quad-polarimetric airborne SAR, elevation and optical RS data." *Remote Sensing of Environment*, Vol. 149: pp. 118–129. doi:[10.1016/j.rse.2014.04.010](https://doi.org/10.1016/j.rse.2014.04.010).
- Van der Linden, S., Rabe, A., Held, M., Jakimow, B., Leitão, J.P., Okujeni, A., Schwieder, M., Suess, S., and Hostert, P. 2015. "The EnMAP-Box—A toolbox and application programming interface for EnMAP data processing." *Remote Sensing*, Vol. 7 (No. 9): pp. 11249–11266. doi:[10.3390/rs70911249](https://doi.org/10.3390/rs70911249).
- Villa, P., Bresciani, M., Bolpagni, R., Pinardi, M., and Giardino, C. 2015. "A rule-based approach for mapping macrophyte communities using multi-temporal aquatic vegetation indices." *Remote Sensing of Environment*, Vol. 171: pp. 218–233. doi:[10.1016/j.rse.2015.10.020](https://doi.org/10.1016/j.rse.2015.10.020).
- Wang, L., Dronova, I., Gong, P., Yang, W., Li, Y., and Liu, Q. 2012. "A new time series vegetation-Water index of phenological-Hydrological trait across species and functional types for Poyang Lake wetland ecosystem." *Remote Sensing of Environment*, Vol. 125: pp. 49–63. doi:[10.1016/j.rse.2012.07.003](https://doi.org/10.1016/j.rse.2012.07.003).
- Wang, C., Menenti, M., Stoll, M.P., Belluco, E., and Marani, M. 2007. "Mapping mixed vegetation communities in salt marshes using airborne spectral data." *Remote Sensing of Environment*, Vol. 107(No. 4): pp. 559–570. doi:[10.1016/j.rse.2006.10.007](https://doi.org/10.1016/j.rse.2006.10.007).
- Wang, D., Wan, B., Qiu, P., Su, Y., Guo, Q., Wang, R., Sun, F., and Wu, X. 2018. "Evaluating the performance of Sentinel-2, Landsat 8 and Pléiades-1 in mapping mangrove extent and species." *Remote Sensing*, Vol. 10(No. 9): pp. 1468. doi:[10.3390/rs10091468](https://doi.org/10.3390/rs10091468).

- Wang, X., Xiao, X., Zou, Z., Chen, B., Ma, J., Dong, J., Doughty, R.B., et al. 2020. "Tracking annual changes of coastal tidal flats in China during 1986–2016 through analyses of Landsat images with Google Earth engine." *Remote Sensing of Environment*, Vol. 238: pp. 110987. doi:[10.1016/j.rse.2018.11.030](https://doi.org/10.1016/j.rse.2018.11.030).
- West, R. C. 1977. "Tidal salt marsh and mangal formations of middle and South America." In *Ecosystems of the World. I Wet Coastal Ecosystems*, edited by V. J. Chapman, 193–213. Amsterdam, The Netherlands: Elsevier.
- Wilcox, D. A. 2002. *Where Land Meets Water: Understanding Wetlands of the Great Lakes*. Downsview, ON: Environment Canada.
- William, D.J., Rybicki, N.B., Lombana, A.V., O'Brien, T.M., and Gomez, R.B. 2003. "Preliminary investigation of submerged aquatic vegetation mapping using hyperspectral remote sensing." *Environmental Monitoring and Assessment*, Vol. 81: pp. 383–392. doi:[10.1023/A:1021318217654](https://doi.org/10.1023/A:1021318217654).
- Wulder, M.A., White, J.C., Loveland, T.R., Woodcock, C.E., Belward, A.S., Cohen, W.B., Fosnight, E.A., Shaw, J., Masek, J.G., and Roy, D.P. 2016. "The global Landsat archive: Status, consolidation, and direction." *Remote Sensing of Environment*, Vol. 185: pp. 271–283. doi:[10.1016/j.rse.2015.11.032](https://doi.org/10.1016/j.rse.2015.11.032).
- Xie, Y., Sha, Z., and Yu, M. 2008. "Remote sensing imagery in vegetation mapping: A review." *Journal of Plant Ecology*, Vol. 1(No. 1): pp. 9–23. doi:[10.1093/jpe/rtm005](https://doi.org/10.1093/jpe/rtm005).
- Xu, H. 2006. "Modification of Normalised Difference Water Index (NDWI) to enhance open water features in remotely sensed imagery." *International Journal of Remote Sensing*, Vol. 27(No. 14): Taylor & Francis: pp. 3025–3033. doi:[10.1080/01431160600589179](https://doi.org/10.1080/01431160600589179).
- Yeo, S., Lafon, V., Alard, D., Curti, C., Dehouck, A., and Benot, M.-L. 2020. "Classification and mapping of salt-marsh vegetation combining multispectral images with field data." *Estuarine, Coastal and Shelf Science*, Vol. 236: pp. 106643. doi:[10.1016/j.ecss.2020.106643](https://doi.org/10.1016/j.ecss.2020.106643).
- Zedler, J., and Kercher, S. 2005. "Wetland resources: Status, trends, ecosystem services, and restorability." *Annual Review of Environment and Resources*, Vol. 30(No. 1): pp. 39–74. doi:[10.1146/annurev.energy.30.050504.144248](https://doi.org/10.1146/annurev.energy.30.050504.144248).
- Zhang, M., L Ustin, S., Rejmankova, E., and Sanderson, E.W. 1997. "Monitoring Pacific Coast salt marshes using remote sensing." *Ecological Applications*, Vol. 7(No. 3): pp. 1039–1053. doi:[10.1890/1051-0761\(1997\)007\[1039:MPCSMU\]2.0.CO;2](https://doi.org/10.1890/1051-0761(1997)007[1039:MPCSMU]2.0.CO;2).
- Zhang, Y., Lu, D., Yang, B., Sun, C., and Sun, M. 2011. "Coastal wetland vegetation classification with a Landsat thematic mapper image." *International Journal of Remote Sensing*, Vol. 32(No. 2): pp. 545–561. doi:[10.1080/01431160903475241](https://doi.org/10.1080/01431160903475241).
- Zhang, X., and Tian, Q. 2013. "A Mangrove Recognition Index for remote sensing of mangrove forest from space." *Current Science*, Vol. 105(No. 8): pp. 1149–1154.
- Zheng, Z., Zhou, Y., Tian, B., and Ding, X. 2016. "The spatial relationship between salt marsh vegetation patterns, soil elevation and tidal channels using remote sensing at Chongming Dongtan Nature Reserve, China." *Acta Oceanologica Sinica*, Vol. 35(No. 4): pp. 26–34. doi:[10.1007/s13131-016-0831-z](https://doi.org/10.1007/s13131-016-0831-z).
- Zomer, R.J., Trabucco, A., and Ustin, S.L. 2009. "Building spectral libraries for wetlands land cover classification and hyperspectral remote sensing." *Journal of Environmental Management*, Vol. 90(No. 7): pp. 2170–2177. doi:[10.1016/j.jenvman.2007.06.028](https://doi.org/10.1016/j.jenvman.2007.06.028).